# Reactions of sub-arc mantle melt with mantle wedge and lower crust

**Swarbhanu Dey**

**School of Natural Sciences**

**Faculty of Science and Engineering**

**Macquarie University, Sydney, NSW 2109**

**December 2, 2022**

**A thesis submitted in partial fulfilment of the requirements for the degree of Master of Research**

# Declaration

This thesis, as a whole or in parts, has not been submitted for a degree or diploma in any university or institution. This work has not been submitted for a higher degree before. I have referenced all sources and the extent to which I used them during the write-up of the thesis. To the best of my knowledge and belief, the thesis contains no material previously published or written by another person except where due reference is made in the thesis itself.

I wish to acknowledge the following assistance with the research detailed in this thesis:

Research for this project was funded by the Australian Research Council Discovery Project funding (ARC- DP200100482) and Stephen Foley's ARC Laureate Fellowship (FL180100134). Stephen Foley and Nathan Daczko supervised this research project. Legacy geochemistry data was compiled from the literature, and legacy samples were provided by Nathan Daczko, Bill Griffin and Chutian Shu. All the samples were prepared for experiments at the high-pressure lab at Macquarie University, Sydney, Australia. Slava Shcheka, Sean Murray, Timothy Murphy, and Yi-Jen Lai provided instrumental and software training. The thesis was reviewed and edited by Nathan Daczko, Stephen Foley, and Aditi Chatterjee. All other research was done by the candidate.

No ethics approval was required for this project.

**Swarbhanu Dey** 2nd December 2022

This thesis is formatted as a manuscript for submission to Lithos, with some exceptions to meet the requirements of Macquarie University. This includes the requirement of an abstract of 200 words, 2 cm margins on all sides, 1.5x line spacing, and figures & tables embedded within the text.

# TABLE OF CONTENTS

# Acknowledgements

During the last nine and a half months, I have spent enjoyable and inspiring time completing my thesis work. Throughout this time, I have acquired a variety of new skills and expanded my horizons in my approaches to geoscience. There are several people I would like to acknowledge and thank for helping and encouraging me. First and foremost are my two great supervisors, Nathan Daczko and Stephen Foley, who facilitated an interesting thesis topic for me to work on. I thank both of you for channelising me at every project step. The time-to-time discussions, suggestions, and feedback resulted in my writing this thesis. Second, I thank Nathan Daczko, Stephen Foley, Bill Griffin and Chutian Shu for providing the samples and necessary information. A special thanks to Macquarie University Geochemical Analysis (MQGA) for allowing me to access all the facilities. I want to mention Sean Murray and Timothy Murphy for helping and advising me at every step of the geochemical analyses. Finally, I appreciate all the people from whom I learnt many new things during my regular visits to the laboratory.

Several academic staff from the EPS department have been of great help at various stages of this project. A heartfelt thanks to Ajay Narendra for designing and smoothly organising the academic programs. I especially thank our regular group meetings for discussing the experimental and geochemical results. It helped a lot!

Acknowledging the warmth and support I received from my colleagues and friends in the department is worthwhile. Thanks to Slava Shcheka, Stephen Foley, and Nathan Daczko for introducing me to the field of research. I want to mention Isra Ezad, Aditi Chatterjee, Joshua Shea and Chutian Shu for time-to-time suggestions and motivation. Also, I thank my friends at Macquarie University. Finally, I am grateful to Slava Shcheka for the assistance and enlightenment he provided at first glance. I thank Yi-Jen Lui, Sean Murray, and Peter Wieland for letting me access the Macquarie Analytical Fabrication Facility (MAFF) and different instruments at Macquarie University.

I am taking this opportunity to express my gratitude to those who have made my stay in Sydney enjoyable during my time here. I thank all the new friends I have made throughout this city and at this university. Ultimately, my heartfelt gratitude goes to my mother, who has always stood by me, supported my decision, and encouraged me to attend Macquarie University.

≈

# Abstract

Most volcanic arc magmas form from the partial melting of mantle wedge above subducting oceanic plates. The melts must migrate through the mantle wedge to reach the arc crust. However, little is known about chemical changes along melt migration pathways. This gap is explored by conducting melt-rock reaction experiments at 1.5 GPa pressure (depth ~50 km), and $1200^0$ C & $1150^0$ C. We used the synthetic primary mantle melt derived from partially melting phlogopite-pyroxenite source rock.

The peridotite rock does not melt at $1200^0$C at 1.5 GPa, but partial melting occurs in phlogopite-pyroxenite components of the mantle. The experiments simulated the flow-through of the partial melts by using a three-layer setup, including a glassy carbon trap at the topmost portion of the capsule, the starting melt at the bottom, which reacts with the peridotite and/or gabbro above it and eventually accumulates within the vitreous carbon trap. This is a novel addition to past experimental designs, improving our ability to analyse the melt composition after reactions with the rock.

Our study aims: (I) to understand the key sub-arc melt-rock reactions, (II) to evaluate geochemical trends resulting from melt-rock interaction under volcanic arcs and determine changes in melt composition, and (II) to compare experimental results with volcanic glass compositions from primitive arcs.

Keywords: Volcanic arcs, phlogopite-pyroxenite, mantle wedge peridotite, lower crustal gabbro, melt-rock reactions.

# Chapter 1: Introduction

Volcanic arcs are initiated when the mantle wedge partially melts over the subducted oceanic slab. In order for melt to reach the crust of the arc, it must migrate through both the mantle wedge and the lower crust. However, the reactions and changes in the melt chemistry along the melt migration pathways are poorly understood. Several studies on the trace elements and isotopes suggest that magmas from the subduction zone boundaries have multiple source petrogenesis (Atherton and Tarney, 1979; Kay, 1980; Green, 1980; Gill, 1981 DePaolo, 1981;). Regardless, the details of the process among the most profound source and the eruption or emplacement of magma still need to be clarified (Hildreth, 1981). Therefore, it is crucial to take into account the interactions of the surrounding peridotite powder with phlogopite-pyroxenite melt to understand partial melting processes in heterogeneous mantle comprehensively. As a result, melt extraction dynamics may be affected, and pyroxenite signatures may be preserved at the surface of aggregated melts. A variety of physical and chemical factors influence the pyroxenite-peridotite interaction process, such as the pyroxenite body size (Kogiso et al., 2004b), the composition of the melts derived from the pyroxenite bodies (Morgan & Liang, 2005), and the nature of the flow mechanism of transportation, such as pervasive porous flow, or focused flows in the dunite channels. The transportation of magma within channels makes it difficult to replicate these processes in a laboratory setting.

The upper portion of the mantle is the potential site which holds a modest amount of pyroxenite of 2.5% (Hirschmann & Stolper, 1996) on the basis of the ratio of the massifs of orogenic peridotite. In the past few decades, petrological, geochemical, and experimental studies have concentrated on the justifications for continental growth as part of a plate tectonic framework, concentrating on high magma volumes generated in continental margins and in island arcs. The subduction of the oceanic crust in the arc environment causes igneous crust and sediments to melt, and those melts travel into the peridotite-rich mantle wedge overlying the subducting slab. The results of these reactions are well established as a hydrous pyroxenite can be obtained from it (Sorbadere et al., 2013). Yet, advance investigation of the next phase of the process is necessary, which is the partial melting of the hydrous pyroxenite and the interaction between the ensuing peridotite and melt further up in the mantle wedge and also in the lower crust.

For melts to reach the arc crust, they must travel through the mantle wedge on their way to the arc crust. On the other hand, the reactions and changes in melting chemistry associated with these melt migration paths need to be better understood. Most petrological models assume an average oceanic crust thickness (Langmuir et al., 1992). Kinzler &

Grove, (1992), predicted an average melting pressure of less than 1.5 GPa for the peridotitic mantle. However, very little is known about the melting behaviour of pyroxenites at P <2 GPa.

In order to investigate this gap, we conduct melt-rock reaction experiments at 1.5 GPa pressure at $1200^0$ C and $1150^0$ C using a rapid quench piston-cylinder apparatus to simulate hybridisation between metasomatized mantle wedge melt ascending from the subducting slab of oceanic crust into mantle wedge peridotite and lower crustal gabbro overlying the mantle wedge peridotite. A harzburgite peridotite and gabbro from the lower crust were selected for experimental reactions with the primary melt. In addition, a glassy carbon trap was placed at the topmost portion of the capsule to collect the experimentally generated melts with new compositions after they migrated and interacted with the overlying rocks. This is a novel addition to past experimental setups. Noble metal capsules ($Au_{80}Pd_{20}$) of about 2.3 mm in diameter and 6 mm in length contain the experiments' samples.

This research investigates the melt flow reactions that occur when melt derived from the partially molten phlogopite-pyroxenite flows through mantle wedge peridotite and lower crustal gabbro above it. Through this study, we define the key melt-rock reactions in the mantle wedge and the lower crust and analyse the chemistry of the newly produced melts. In addition, we observe and compare the geochemical trends associated with melting beneath the arc crust and in global volcanic arc settings. These experiments simulate the reactions between a hydrous siliceous magma into an overlying harzburgite peridotite and gabbro layer, representing the mantle wedge above the subducting slab and the lower crustal composition.

# Chapter 2: Literature Review

The pyroxene lithologies in oceanic basalts have been studied extensively through a combination of experimental (Kogiso et al., 2004a) and geochemical (Le Roux et al., 2002; Sobolev et al., 2007) investigations. However, even though pyroxenites make up a much smaller part of the upper mantle than peridotite, they are likely to account for a substantial amount of melt production since they have a low temperature of solidus and a high productivity of melt (e.g., Hirschmann & Stolper, 1996; Pertermann & Hirschmann, 2003; Lambart et al., 2009).

## *2.1. The processes within the mantle wedge*

### *2.1.1. Fluid infiltration and partial melting of the mantle wedge*

Several studies in early and active subduction zones indicate that some fluids released from the subducting plates migrate upwards into the mantle wedge directly above the slab. This migration occurs during subduction. The serpentinite diapirs have been said to be the result of the hydration of the mantle wedge directly above the subducting plate during the subduction process. It has been observed that at the pressures between 5 to 10 kbar, melts derived from subducted sediments and basalts layers and the mantle wedge produce hydrous carbonates and hydrous silicates (Talc, Mg-amphibole, and Serpentine) in the Trinity thrust system (in Northern California), and Catalina Schist terrane (in Southern California). Aside from the dissolved chemical species carried by the infiltrating $H_20$-$CO_2$ fluids, the mantle wedge also absorbed $SiO_2$, and CaO dissolved within it, thereby changing its bulk composition. Metasomatic effects in the mantle wedge regions are observed on the basis of the composition of island arc basalts, which reflect the mantle sources that generated those basalts. In comparison with the Mid Ocean Ridge Basalts (MORB), the arc-basalts have a depletion of high-field strength elements, such as Zr, Ti, and Nb, compared to the large ion lithophile elements LILE: K, Sr, Ba, and light rare earth LREE. The presence of such imprints is associated with the MORB-type mantle melting enriched in LILE relative to HFSE after equilibration with metasomatic agents escaping the subducting oceanic crust (e.g., Brenan et al., 1994; Kelemen et al., 1993).

### *2.1.2. Depths of fluid release*

It has been determined from geophysical data that the slab lies at depths of 100 to 150 kilometres beneath arc volcanoes, according to Gill 1980. During the late 1980s and early

1990s, a study of the dehydration of the subducting oceanic crust revealed the appearance of a significant fluid pulse at relatively constant depths between 70 and 80 kilometres, roughly coinciding with the depth of the decomposition of amphibole (e.g., Tatsumi, 1989; Davies & Bickle, 1991). Few early experimental studies have also demonstrated that other hydrous phases such as phengite, lawsonite, antigorite, chloritoid, zoisite-clinozoisite, and staurolite have the ability to carry water much greater depth than amphibole (Wunder & Schreyer, 1992; Schreyer, 1988; Pawley & Holloway, 1993; Ulmer & Trommsdorff, 1995; Poli & Schmidt, 1995; Schmidt, 1996; Schmidt & Poli, 1998).

## *2.2. Formation of calc-alkaline igneous rocks at converging plate boundaries*

There is growing consent today that calc-alkaline igneous rocks originated at the convergent plate boundaries through complicated multisource processes that also involved additional fractionation effects (Atherton & Tarney, 1979; Green, 1980; Kay, 1980; Gill, 1981; DePaolo, 1981; Wyllie, 1981; Hildreth, 1981). Several studies have been conducted on the petrology of subduction zones, the formation of the calc-alkaline igneous rocks at the convergent plate boundaries, and mantle hybridisation. Mantle hybridisation is a phenomenon that occurs when a mixture of two melts or a solid combined with another melt is produced, thus producing a secondary composition (Durocher, 1857).

Several papers were published by Sekine and Wyllie on hybridisation in subduction zones; As an example, Sekine and Wyllie (1982a) studied the data present in the $KAlSi_3O_8$-$SiO_2$-$H_2O$ system, including two types of eutectic liquids (1) fluids containing silica hydrates from subducted ocean crust and (2) forsterite and enstatite assemblages derived from oceanic crust overlying mantle in the system $Mg_2SiO_4$-$SiO_2$-$H_2O$.

Besides the experiments done by Sekine and Wyllie in 1973, Yoder conducted two experiments with granite and pounded basalt separated by a vertical interface at 1 kbar with excess $H_20$ at 1200° C and 950° C, respectively. It was observed that when the glass was heated to 1200° C, the colourless and brown glass had a sharp interface separating them. Additionally, it was observed that colourless glass separated from recrystallised basalt at a sharp interface at around 950° C, and the flow of granite liquid around the basalt cake's end. On an interface similar to this at 1200° C (with different materials), electron microprobe analyses revealed a zone of diffusion that spanned 300 μm, with the majority of the modifications taking place within 60 μm (Yoder, 1973).

In the past, there has been an increasing number of studies supporting the possibility of convergent plate boundary magmas generated by multisource petrogenesis (Atherton &

Tarney, 1979; Kay, 1980; Green, 1980; Gill, 1981; DePaolo, 1981; Hildreth, 1981). For instance, the Yunshan Fold & Thrust Belt in eastern China has been intruded by a series of alkaline igneous rocks which has a compositional ranges from granite to trachyte. Three rocks have been identified on the basis of mineralogical, geochemical composition and Sr-Nd–Hf isotopic characteristics. Most of the rocks are composed of iron oxides, which contain low amounts of MgO, $Al_2O_3$, CaO, Ba, Sr, and Eu, but high amounts of $Fe_2O_3$, $SiO_2$, $K_2O$, Ga, Nb, Ta, and heavy rare earth elements (HREEs). Geochemical analysis of these rocks and their Nd, Sr, Zr and Hf-isotopic compositions strongly suggest that they originated from shallow dehydration melting of granitoid crustal rocks containing biotite or hornblende, followed by mixing with contemporary magma from the mantle or lower crust. The geochemical makeup of ferroan syenites differs from the alkaline granites and rhyolites, which are formed by the fractionation of mantle melt from an enriched source mixed with lower and upper crustal magmas (Yang, J. H. et al. 2008). However, details of the processes between the most profound origin and magma eruption or emplacement remain unknown. Therefore, the hybridisation hypothesis should be tested considering the attention dedicated to the simple forward and inverse approaches.

## *2.3. Key steps in the generation of calc-alkali fractionation trends*

A long and complicated history has been associated with the term 'calc-alkaline' (Arculus, 2003). In 1909, Harker identified two types of volcanic rocks: the Pacific Branch (which contains a greater amount of magnesium oxide and calcium oxide) and the Atlantic Branch (which contains a greater amount of alkali). Holmes (1918) observed that at 62 wt% $SiO_2$ for Pacific Branch-type calc-alkaline igneous rocks, there is a cross-over between the $SiO_2$-CaO and $SiO_2$-alkalis ($K_2O$+$Na_2O$) trends. As a result of the intersection of both alkali and caustic trends, Peacock (1931) defined a 'calc-alkalic' group (intersection at 56-61 wt% $SiO_2$) based on the value of $SiO_2$ at which the two trends intersected. This characterisation guides to the term "calc-alkaline", but it has shifted away from this concept. The magma produced in subduction zones exhibits several evolutionary trends, such as noticeable depletion in iron ( Fenner, 1926, Rose & Chesner, 1984; Kay & Kay, 1985; Grove et al., 2003; Carr et al., 2003.). Also, the depletion in iron has been reported in ocean island basalts (OIB) ( Munoz Garcia, 1969; Ibarrola Munoz, 1970; Thirlwall et al., 2000 ) and also in the continental rift magmas (Trua et al., 1999; Wang et al., 2002; Krienitz et al., 2007 ).

The calc-alkaline trends of Fe depletion can be generated in several ways, depending on the conditions. In consequence, low-content of water ( Grove & Baker, 1984; Baker & Eggler,

1987; Kinzler & Grove, 1992; Sisson & Grove, 1993a; Grove et al., 2003 ) or reduced crystallisation pressure ( Gust & Perfit, 1987; Kinzler & Grove, 1992 ) decreases the possibility of plagioclase crystallisation in aqueous solutions (Grove & Baker, 1984). Some hypotheses of the origin of calc-alkaline trends involve calcification of Fe-rich phases, like magnetite ( Osborn, 1959; Gill, 1981; Sisson & Grove, 1993a, 1993b ), or calcification of amphibole ( Cawthorn & O'Hara, 1976; Grove et al., 2003 ). It is also possible that calc-alkali trends can result from the assimilation and mixing of silicic melts with a low Fe content ( Grove & Baker, 1984; McBirney et al., 1987; George et al., 2004 ) or from mantle melt reactions (Kelemen, 1990). Generally, arc magma can be defined as a combination of mantle material with one or more additional materials added to it (e.g., Gill, 1984; Hawkesworth et al., 1991).

The calc-alkaline trend is stronger in the line of descent (LLD) when magnetite crystallises earlier, an effect that is not reproduced by *pMELTS* ( Ghiorso & Sack, 1995; Ghiorso et al., 2002 ), even though there is strong experimental evidence to the contrary. It is believed that water depolymerises silicates; the more complex the silicate structure, the greater the level of depolymerisation, thereby allowing oxide crystallisation to occur. Based on the experimental data, it has been shown by Sisson & Grove (1993a) that a phase of spinel may emerge on the basalt liquidus with 3.5 to 6.0% $H_2O$ at ~NNO (nickel-nickel oxide).

## *2.4. Experimental approaches to the subduction zonegeochemistry*

At destructive plate boundaries, crustal recycling seems to be a rudimentary mechanism for maintaining the geochemical heterogeneity of the mantle (Armstrong, 1968; Chase, 1981; Hofmann & White, 1982; Allègre, 1982; Ringwood, 1982; Zindler & Hart, 1986; Hofmann, 1997; Stracke, 2012). Consequently, the radiogenic isotope and trace elemental composition in subduction zone magmas are determined mainly by the transfer of elements from the subducting crust to the overlying mantle wedge (e.g., McCulloch and Gamble, 1991; Woodhead et al., 1993; Tatsumi & Eggins, 1995; Turner & Hawkesworth, 1997; Stern, 2002; Spandler & Pirard, 2013; Kelemen et al., 2014; Zheng & Chen, 2016). Furthermore, several studies suggest that intraplate basalts can be utilised to study the geochemical signatures of subducting oceanic crust (Sun, 1980; Allègre, 1982; Zindler & Hart, 1986; Sun & McDonough, 1989; Hofmann, 1997; Stracke, 2012; Farmer, 2014; Zhao et al., 2015; Huang & Zheng, 2017; Xu & Zheng, 2017). In spite of the fact that the most important inputs during subduction can be traced through volcanic outputs, considerable uncertainty remains regarding the nature of element transfer from forearc depths of 60 to 80 km to sub-arc depths of 80 to 160 km to back-arc depths of > 200 km. In order to determine the dehydration behaviour of the

subducting crust and the elemental mobility at different depths, many geochemical investigations have been carried out. In general, these studies can largely diverge into two classifications: (a) The first class deals with igneous rocks of mafic composition (Elliott et al., 1997; Tatsumi & Kogiso, 1997; Churikova et al., 2001; Regelous et al., 2010; Cai et al., 2014; Kelemen et al., 2014; Ryan & Chauvel, 2014), (b) Other investigations have mostly focused on the high pressure (HP) or ultrahigh-pressure (UHP) metamorphic rocks (Zhao et al., Tribuzio et al., 1996; Becker et al., 2000; Zack et al., 2001; Spandler et al., 2003, 2004; Bebout et al., 2007, 2014; Gao et al., 2007; Miller et al., 2007).

Pyroxenite-peridotite interactions are influenced by a variety of physical and chemical parameters, for example, the body size of pyroxenites (e.g., Kogiso et al., 2004b), the composition of the melts obtained from a pyroxenite body (Morgan & Liang, 2005), and the transport mechanisms of the melt (such as porous pervasive flow and the focused flow within the dunite channels, and transport of magma in dikes). Hence, simulating these methods in the laboratory is difficult and takes a lot of time. Nonetheless, several experimental studies have been conducted to study how silicate melts interact with peridotites from a chemical point of view to understand the process better. The kinetic studies conducted by Morgan & Liang (2003, 2005) in different types of open reactors, where a large amount of matter is exchanged with the surroundings and which is responsible for the exchange of matter on interactions between basaltic melt and peridotite, demonstrate that the exchanges between the two substances are kinetic. As a function of the melt composition, it was observed that some modifications were made to the peridotite assemblage that was more or less significant.

Nevertheless, it is not easy to compute the interactions and their effect on the melt and the composition of peridotite in this kind of disequilibrium experiment. For example, in 'sandwich experiments', Yaxley & Green (1998) and Pilet et al. (2008) packed a layer of matter with a low-solidus temperature within the layers of the peridotite. As a comparison, Yaxley & Green (1998) employed a MORB-type eclogite and presented their experiments at the pressure of 3·5 GPa, whereas Pilet et al. (2008) utilised hornblendite at 1·5 GPa pressure. As opposed to experiments performed by Morgan & Liang (2003, 2005), most of the reaction experiments were done below the peridotite's solidus temperature, simulating a partially molten pyroxenite body in a sub-solidus host. There is an opposite conclusion to be drawn from the two studies of Yaxley and Pilet and Morgan and Liang, which conclude that melts from a source contribute to the formation of orthopyroxene (Opx), whereas melts from a source dissolve Opx from the neighbouring peridotite and precipitate olivine (Ol). The experimental studies of Yaxley & Green (1998) and Pilet et al. (2008) deal mainly with the

impact of melt-rock reaction on the melt composition. However, comparing their findings highlights the significance of the reaction's primary conditions, such as pressure and composition. Likewise, it demonstrates that the melt-rock reactions may greatly impact the mantle's lithological diversity. This study aimed to evaluate how melts from pyroxenite sources behave during their transportation through the mantle wedge peridotite as a function of their composition, P-T conditions, and the physical state (sub-solidus *vs.* partially molten) of the surrounding mantle during their transportation. This study examined three cases to assess how melt-rock interactions affect melt chemical composition, the surrounding peridotite's chemical and mineralogical compositions, and the melt's ability to penetrate the rocks.

For example, Garrido & Bodinier (1999) proposed that some pyroxenites of the Ronda Massif (SW Spain) originated as a consequence of an interaction between the melt of alkali basalt and peridotite. An important characteristic of the reaction between the pyroxenite derived melts, and host peridotite is the simultaneous dissolution of Opx and the precipitation of olivine that occurs. It is possible to describe this reaction by a simple equation such as:

$$Opx + Liq_0 \leftrightarrow Ol + Liq_1$$

When liquid, Olivine, and Opx are the only phases present in a simple system at constant pressure & temperature, the experimental (Daines & Kohlstedt, 1994) & thermodynamic (Kelemen, 1990) studies have indicated that the proportion of precipitated olivine to dissolved Opx, $M_{Ol}/M_{Opx}$ is $\sim$7. As a result, Opx dissolution and Olivine precipitation raise the proportion of melt in the system and accelerate its transport by enhancing the porosity and the permeability of mantle rocks. Alternatively, Opx crystallisation employing olivine dissolution may cause a decrease in porosity, which may slow down or even stop magma ascent through porous flows. In this case, interactions between basalt and peridotite may substantially influence the rate at which magma is transported from its source region to the surface.

Several petrological processes occur in the supra-subduction mantle, from dehydration in the subducted plate to partial melting and metasomatism in the wedge. In addition, these processes can significantly influence mantle peridotites' composition, rheology, and flow pattern. As an example, it has been demonstrated that melting fractions and water in the olivine can lower the strength of the mantle rocks (Blacic, 1972; Boudier, 1991; Demouchy et al., 2012; Hirth & Kohlstedt, 1995a; Hirth & Kohlstedt, 1995b; Mackwell et al., 1985; Karato et al., 1986; Mei & Kohlstedt, 2000a; Mei & Kohlstedt, 2000b; Mei). Furthermore, seismic anisotropy and mantle flow can be influenced by changes in plastic deformation mechanisms in olivine (Jung & Karato, 2001; Holtzman et al., 2003b). However, several experiments have found that melting. Percolation in peridotite massifs and xenoliths may be responsible for this effect, which enhances

pyroxene crystallisation and disturbs olivine crystal preferred orientations (CPO), reducing seismic anisotropy in peridotites (Le Roux et al., 2008; Soustelle et al., 2009; Soustelle & Tommasi, 2010; Soustelle, 2014).

## *2.5. The review of past and current petrogenetic models*

Grove et al. proposed in 2003 that calc-alkali magma fractionates via dehydration of hydrous minerals and vapour-saturated anatexis (marked I, Figure 2.1) porous flow process (flux melting). This results in a melt traversing an inverted thermal gradient in a hotter shallower mantle. With a decrease in equilibration pressure, silicate minerals dissolving in the melt also lead to a reduction in the amount of water in the melt. Additionally, this process continues to shallow mantle depths (IV, Figure 2.1) as the hydrous melt is segregated (Grove et al., 2002; Grove & Gaetani, 2003). Grove and Gaetani (2003) found that the mantle was melted significantly (> 20 wt%) by this flux-melting model, causing a dilution of slab-contributed trace elements and fluids. Recently, studies have focused on the mechanisms explaining continental expansion within a plate tectonic framework, particularly in continental margins and island arc regions. As a result of geochemical studies on island arcs (Sakes and Gill, 1969; Gill, 1970; Jakes & White, 1971), the earlier view that andesite (~60% $SiO_2$) dominates active orogenic areas has been replaced with three rock series (Sakes and Gill, 1969; Gill, 1970; Jakes & White, 1971):

(a) Island arc tholeiitic series (dominant).
(b) Calc-alkaline series.
(c) Island arc alkaline (or shoshonitic) series (smallest abundant).

According to Middlemost (1985), determining the alkali-lime index of a standard suite of rocks containing orogenic andesites shows that some of the rocks are more likely to belong to the calcic series of Peacock rather than to the calc-alkalic series. Middlemost (p. 118) also noted that the basalt-Icelandic suite of rocks in the "tholeiitic" group usually falls within the "calc-alkaline" group.

To examine the hypothesis that calc-alkaline rocks of subduction zones are the resultof the partial melting of hybrid rocks formed by the reactions between hydrous siliceous magma rising from subducted oceanic crust and adjacent peridotite, Sekine and Wyllie used granite and peridotite under pressures of 30 kbar. As a result of hybridisation, a pyroxenite. without olivine is produced The products obtained from the partial melting of this composition would be completely different from those made

from peridotite because there is no olivine present, and clinopyroxenes may contain up to 7% $Na_2O$, whereas peridotite has little $Na_2O$. Some scientists favour complex multi-source and fractionation processes, with multi-source processes being superimposed (Atherton and Tarney, 1979; Kay, 1980; Green, 1980; DePaolo, 1981; Hildreth, 1981; Gill, 1981; Wyllie, 1981) as Nicholls and Ringwood proposed (1973), the subducted crust and the overlying mantle are both involved in this process. Based on the results of this study, a hydrous siliceous melt of a similar composition to rhyodacite was formed in the oceanic crust and reacted with the peridotite overlying them. A second stage in the petrogenesis of andesites and other calc-alkaline magmas involving hybridisation was proposed by Nicholls and Ringwood in 1976, in comparison with the previous study conducted in 1973. They suggested that, in subducting oceanic crust, hydrous siliceous melts with solidification characteristics similar to rhyodacites formed, then reacted with mantle peridotite, forming olivine pyroxenite zones. In this zone, olivine pyroxenite accumulates episodically with subsequent partial melting and the formation of calc-alkaline magmas emanated from a variety of these wet, hybrid rocks.

The recent study of the internal structure of the mantle wedge, conducted by Turner et al. (2016), indicates that magma composition correlates with the depth of the Moho concentration zone under the arc. Alternatively, to the depth of the slab under the arc and the slab surface temperature, a slab 'thermal parameter' can be used to define the thermal structure of the down-going slab.

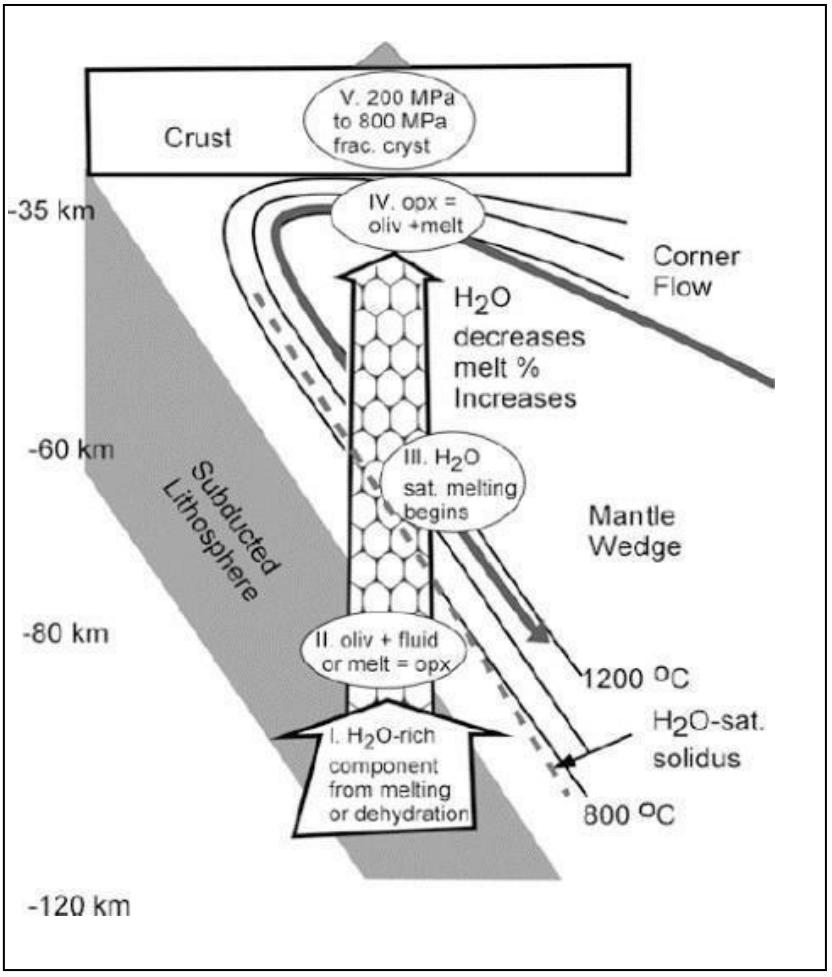


*Figure 2.1: A multi-stage slab melting model was proposed by Grove et al., 2003 as an alternative to explaining the major and trace elements in these lava flows. As a consequence of flux melting, these magmas inherited the main element characteristics of a mantle wedge and progressed upward. Because of this, the melt is rich in $SiO_2$, MgO, and $H_2O$ and saturated with harzburgite. In fractional crystallisation under hydrous conditions, liquid derivatives rich in $SiO_2$ followed calc-alkaline differentiation patterns. Moreover, a fluid component rich in $H_2O$ and trace elements was released into the atmosphere during subduction. Upon melting, this component played a significant role (Grove et al., 2002).*

In light of the new geochemical and experimental studies conducted in island arcs and continental margin areas, the petrogenetic models have been modified to make clear these geochemical and experimental results. In spite of the fact that most of the present models emphasise polygenetic origins for magma series, seawater from the subducted oceanic crust is released into the subducted lithosphere through dehydration and possibly melting reactions. However, there is an alternative explanation for the low $TiO_2$ levels; early melting episodes may have depleted the mantle and resulted in a heterogeneous mantle (Ringwood, 1975; D.H. Green, 1973, 1976). The present models can be grouped into four large categories:

(A) Hydrous melting of peridotite above the Benioff Zone to form liquids at depths of 60 to 100 km, ranging in composition from olivine-tholeiite-quartz tholeiite, which produces basaltic andesite upon rising to the surface (e.g., Nicholls & Ringwood, 1973); and andesite-dacite (e.g., Kushiro,1972).

(B) Melting of the subducted oceanic crust of eclogite mineralogy at depths of 100 to 200 km to produce (1) intermediate rocks belonging to the calc-alkaline series (i.e., primarily andesite) (e.g., T.H. Green and Ringwood, 1968; T.H. Green, 1972; Marsh & Carmichael, 1974); (2) very siliceous liquids (rhyodacite), which rise and "contaminate" and eventually lead to the melting of mantle peridotite (Ringwood, 1974, 1975; Nicholls, 1974),

(C) Hydrous fractionation of mantle derived mafic magma that ranges in composition from alkaline to tholeiitic (e.g., Cawthorn et al., 1973; Arculus, 1976) or both (e.g., Cawthorn & O'Hara, 1976), and

(D) A silicic volcanic and plutonic formation can be produced in mature island arcs and continental margins when thickened crust melts due to the advent of fluids from the Benioff Zone lowering the solidus and heating the crust due to underplating by lavas generated by mechanisms (A) and (B) (D.H. Green, 1972; Ringwood, 1974). Furthermore, magma mixing and contamination are also likely to play a crucial role in this type of environment (e.g., Wilcox, 1954; Anderson, 1976; Eichelberger, 1974).

# Chapter 3: Methodology

We conducted a series of reaction experiments to determine the key melt-rock reactions and to understand how the chemistry of melt changes during the melt migration through the mantle wedge and lower crust beneath the volcanic arc system. In these experiments, we used a rapid quench piston-cylinder instrument with a standard cell assembly, including MgO inner sleeves, graphite furnaces, and Pt-Rh thermocouple wires of type B. All experiments were conducted with a standard $CaF_2$ cell assembly, and no pressure corrections were required. Besides, a partial melt of homogeneous phlogopite-pyroxenite was synthesised in the laboratory for melt flux reaction experiments.

## *3.1. Materials and method*

### *3.1.1. Sample preparations*

Each experiment comprised three layers: (1) melt, (2) rocks in powdered (harzburgite peridotite and dry gabbro) and core form (dry gabbro), and (3) a vitreous carbon melt trap.

(1) Partial melt from a homogeneous phlogopite-pyroxenite was produced synthetically (details of the chemistry are presented in Table 3.2) using 16 major oxides and 21 trace elements. The synthetic melt was mixed and sintered at 950 $^0$C in a furnace and stored in an oven to keep dry.

(2) Two well-characterised rocks were powdered: (a) natural harzburgite peridotite rock from Kimberley, South Africa (sample and data are provided by Bill Griffin, Table 3.1) and (b) natural gabbro rock from Days Creek of the New England Orogen, NSW, Australia (sample provided by Nathan Daczko). Two experiments have been done with the initial melt and lower crustal gabbro. One experiment was between the melt and gabbro in the form of powder (crushed into the size of 15 – 20 μm), and another reaction experiment was run using a rock core drilled from the gabbro instead of powder. The core was cut down into 2.2 mm x 2.6 mm from the same gabbro.

(3) 10–20 micrometre (μm) sized vitreous carbon beads were used to create porosity at one end of the experiment.

## *3.2. Experimental design and analytical techniques*

### *3.2.1. Experimental setup*

A half-inch-diameter rapid quench piston-cylinder apparatus was used to react sealed samples

at 1.5 GPa pressure. To achieve the target temperature, a type B thermocouple was used for each experiment, with a positive leg made up of 70% of Pt and 30% of Rh and a negative leg made up of 94% of Pt and 6% of Rh.

In order to study melt-rock reactions, mantle wedge peridotite and lower crustal gabbro were selected for our study. We have begun our reaction experiments using a 1.5×6 mm $Ag_{70}Pd_{30}$ metal capsule (Figures 1 & 2, Appendix) to minimise iron loss during high-pressure experiments. Subsequently, we employed a 2.3×5 mm $Au_{80}Pd_{20}$ metal capsule (Figure 3.1A) to conduct the high-pressure experiments. As shown in Figure 3.1A, the melt was placed in the capsule on the bottom end, the peridotite in the middle, sandwiched between the vitreous carbon layer and the melt, and the vitreous carbon melt trap on top (Figure 3.1B). This same experimental design was applied to gabbro powder as well as to the gabbro core (Figure 3.1 C), in which melt migrated through both. After each experiment, all capsules were mounted in epoxy resin and polished with different grits of sandpaper to a diamond finish of 1/4 m.

Melt traps are primarily used to collect the new melt after each reaction with overlying rocks within the capsule; this is a novel addition to the previous experimental design to improve our ability to analyse the melt composition. The pore spaces within the carbon trap initially offers a lower pressure than elsewhere in the capsule. Melt movement had to occur against gravity as experiments were conducted with a melt trap at the top of the capsule. The proportion of vitreous carbon trap to silicate melt was kept low to allow complet filling of the pores with melt and subsequent melt equilibration. In this manner, the melt can reach equilibrium within a few hours, avoiding problems with achieving equilibrium, which can occur when the pore space of the trap is too large. In our study, all the experimental reactions happened for more than 24 hours. The capsules were heated at $110^0$ C for more than 30 minutes to test for leaks after welding and reweighed. The details of the experiments are presented in Table 4.1 and discussed in the results chapter and table 1 in the appendix.

### *3.2.2. Analytical techniques*

The minerals and microstructures were identified with high resolution using backscattered electron images. An FEI Teneo Field Emission Scanning Electron Microscope (SEM) with NanoMin software (Figures 3 & 4, Appendix) was used for chemical field mapping, and a Zeiss EVO MA15 SEM with Aztec Software was used for microchemical data analyses at Macquarie Geo-Analytical, Macquarie University, to image polished, mounted and carbon coated sections of the samples. The SEM operating conditions were a high vacuum, 10 kV accelerating voltage, a dwell time of 5 ms and spot sizes between 30-50µm. For each sample, stitched images of

the thin sections were uploaded as layers to ImageMatrix. This software helps compile the individual major oxide's concentration map onto a BSE image (See Au-Pd Zeiss SEM - Files - CloudStor (aarnet.edu.au)). Additionally, they were used to identify different minerals and chemical phases and their distribution in the studied samples.

A laser ablation inductively coupled plasma mass spectrometry (La-ICP-MS) analysis was performed at the Macquarie Analytical & Fabrication Facility (MAFF) of Macquarie University to determine the trace elemental concentrations in melts. The instrument consists of an Agilent 7700 mass spectrometer coupled to a New-Wave Research UP213 Md- YAG (213 nm) laser. The analysis was conducted by ablating 30 µm diameter spots at a rate of ten shots per second. The data reduction process was completed based on a standard methods (Longerich et al., 1996), utilising STD610 and STD612 glasses as the primary references and USGS BCR2g glass as a secondary reference. The details of the analyses are presented and discussed in the results chapter (Under section 4.4: Trace elemental analyses).

| **Oxides** | **KF 06-002** |
|---|---|
| $SiO_2$ | 46.07 |
| $TiO_2$ | < 0.01 |
| $Al_2O_3$ | 1.22 |
| $Fe_2O_{3(TOTAL)}$ | 6.02 |
| MnO | 0.09 |
| MgO | 42.02 |
| CaO | 0.43 |
| $Na_2O$ | <0.02 |
| $K_2O$ | 0.02 |
| $P_2O_5$ | <0.01 |
| $Cr_2O_3$ | 0.37 |
| LOI | 4.22 |
| Sum | 100.46 |

*Table 3.1: Chemistry of natural harzburgite powder from Kimberley, South Africa (Sample and data provided by Bill Griffin).*

| Chemicals | Melt | Normalised to 100 | Added as | Calculated amount (1 g) |
|---|---|---|---|---|
| $SiO_2$ | 38.00 | 40.58 | The amount from $Fe_2SiO_4$ | 0.02840 |
| | | | $SiO_2$ | 0.37742 |
| $TiO_2$ | 3.29 | 3.51 | $TiO_2$ | 0.03514 |
| $Al_2O_3$ | 7.48 | 7.99 | $Al(OH)_3$ | 0.12224 |
| $Cr_2O_3$ | 0.09 | 0.10 | $Cr_2O_3$ | 0.00096 |
| FeO | 6.36 | 6.79 | $Fe_2SiO_4$ | 0.09633 |
| MnO | 0.10 | 0.11 | MnO | 0.00107 |
| MgO | 10.97 | 11.72 | MgO | 0.06514 |
| | | | the amount from $Mg(OH)_2$ | 0.05202 |
| CaO | 8.09 | 8.64 | $CaCO_3$ | 0.15420 |
| BaO | 0.50 | 0.53 | $BaCO_3$ | 0.00687 |
| $Na_2O$ | 1.34 | 1.43 | $Na_2CO_3$ | 0.00690 |
| | | | the molar Na from NaF | 0.00033 |
| $K_2O$ | 10.58 | 11.30 | $K_2CO_3$ | 0.16578 |
| F | 0.59 | 0.63 | NaF | 0.01393 |
| $H_2O$ | 5.50 | 5.50 | $Mg(OH)_2$ | 0.02168 |
| | | | the amount from $Al(OH)_3$ | 0.04236 |
| Trace elements | 1.17 | 1.17 | Trace | 0.01170 |
| Sum | 87.39 | 100.00 | Total | 1.20246 |

*Table 3.2: Calculation of synthetic melt of homogeneous phlogopite-pyroxenite as starting material.*

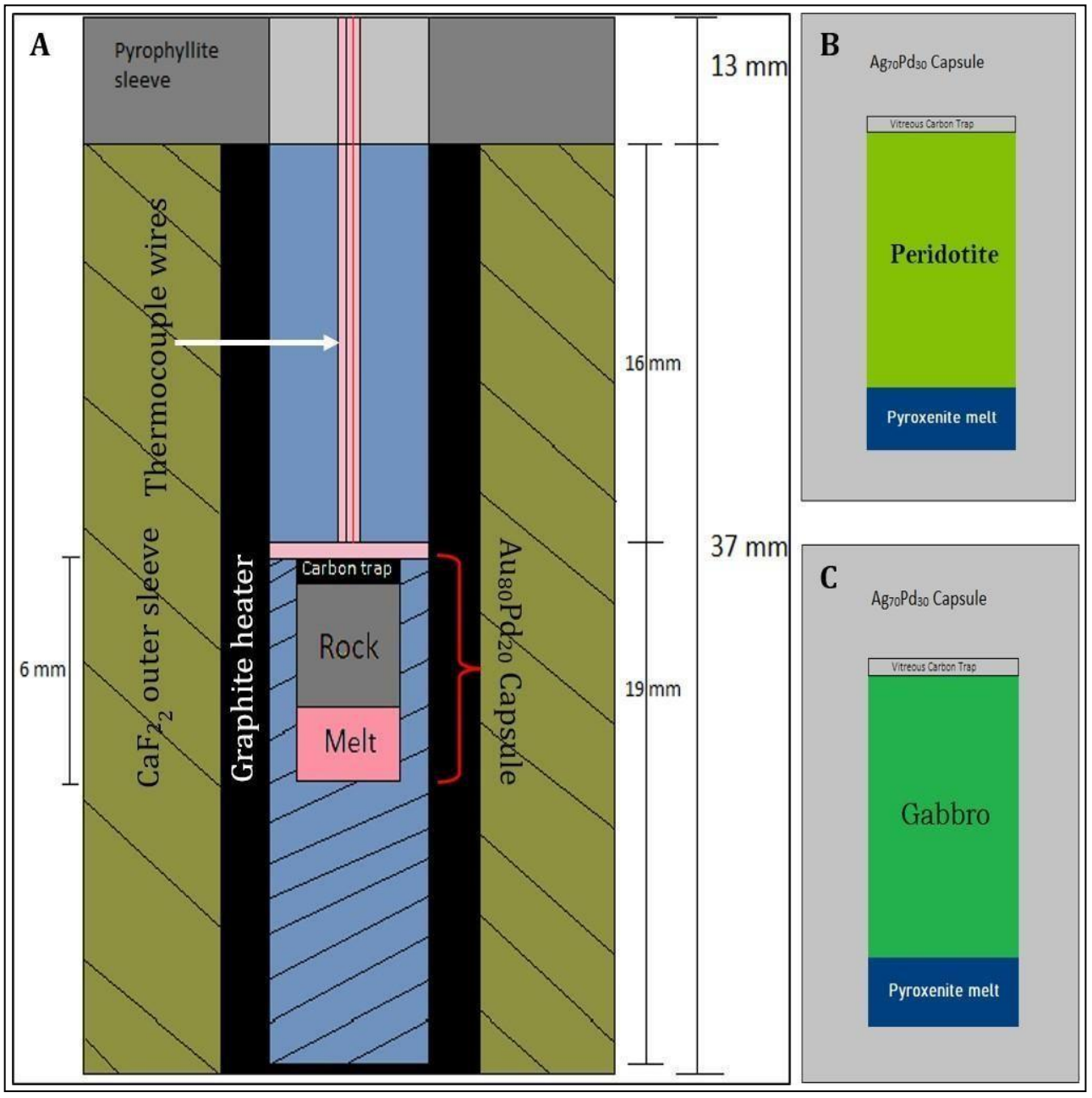


*Figure 3.1: (A) The design of capsules ($Au_{80}Pd_{20}$) used in the experiments. Dark lime is the $CaF_2$ outer sleeve portion. Black coloured portion is the graphite heater sleeve. Pale blue is MgO inner sleeve. The capsule consists of three distinct layers. The top layer is composed of a vitreous carbon trap, the middle portion is composed of rock (powder as well as core), and the bottom part is composed of the synthetic partial melt of a phlogopite-pyroxenite. The vitreous carbon trap forms a low-pressure sink to draw the melt through the rock. (B) The design of capsules for experiments. Peridotite is packed below peridotite as separate layers, so the melt must flow against gravity, sucking through the vitreous carbon melt trap. (C) Design the design of capsules for experiments. Gabbro is packed below peridotite as separate layers, so the melt has to flow against gravity, sucking through the vitreous carbon melt trap.*

# Chapter 4: Experimental Results

## *4.1. Melt-rock reactions in the mantle wedge*

### *4.1.1. Melt-Peridotite reaction*

At the pressure of 1.5 GPa and $1200^0$ C (Table 4.1), we react the initial melt (Table 4., column 1) with the mantle wedge peridotite (Figure 4.1 a-c). As a consequence of the melt-rock reactions, forsterite olivine was produced (Figure 4.1b), with new orthopyroxene (Figure 4.1b & 4.2a), phlogopite (Figure 4.1c) and the composition of the initial melt modified into a new composition (Figure 4.1a, Table 4.2). This experimentally produced new melt is enriched in MgO, $SiO_2$, MnO and $Cr_2O_3$ and depleted in FeO, $Al_2O_3$, $K_2O$ and $Na_2O$ (Table 4.2).

## *4.2. Melt-rock reactions in the lower crust*

### *4.2.1. Melt-Gabbro powder reactions*

During the melt-rock reaction experiments, the migration of the starting melt through the overlying gabbro powder layer forms new orthopyroxene minerals of second-generation as rims surrounding the first-generation clinopyroxene (Figure 4.1e, g and h, & figure 4.2c-f), second-generation labradorite plagioclase (Figure 4.1e-f, and Figure 4.2b), new garnet (Figure 4.1f & h, and Figure 4.2g-h), and a melt of new composition (Figure 4.1d & g). This new melt is enriched in $Al_2O$, $SiO_2$ and alkali oxides and depleted in MgO and FeO (Table 4.2).

### *4.2.2. Melt-Gabbro core reactions*

At 1.5 GPa pressure and $1150^0$ C (Table 4.1), the initial melt reacted with lower crustal dry gabbro (in core form). The mineralogy of the sample (Figure 4.1, g- i) is diopside, enstatite, plagioclase and garnet and a melt with new chemical compositions (Table 4.2, column 4). This melt is very similar to the melt produced during the reaction with the gabbro powder. This melt is also enriched in $SiO_2$, $Al_2O_3$ and $Na_2O$ and depleted in MgO, FeO, MnO, CaO, $Cr_2O_3$ and $K_2O$ (Table 4.2, column 4). During the melt-rock reaction, the partial melt reacted with the gabbro and produced orthopyroxene (enstatite) (Figure 4.1 g & 4.2 B and Table 4.4) of the second-generation; on the other hand, clinopyroxene composition (diopside) (Figure 4.1 h & 4.2 A and Table 4.3) remained the same. Melt reacted with clinopyroxenes and formed rims of orthopyroxene surrounding the clinopyroxene cores of the first-generation, the same as the

melt-gabbro powder reaction. The melt also reacted and formed second-generation plagioclase feldspar of labradorite in composition (Figure 4.1 h, 4.2 C & Table 4.5). Garnet was produced (Figure 4.1. h & 4.2. D and Table 4.7) along the melt migration path during the melt-rock reactions.

| Experimental ID | Material used | Pressure | Temp. | Run Length | Phases occurred |
|---|---|---|---|---|---|
| M-22-054 | Capsule- $Au_{80}Pd_{20}$ Pyroxenite+ peridotite+ vitreous carbon trap | 1.5 GPa | 1200º C | 29 Hours | Rich in olivine, diopside, phlogopite and new melt. Rock minerals that have recrystallised include Mg-olivine (forsterite). |
| A-22-079 | Capsule- $Au_{80}Pd_{20}$ Pyroxenite+ gabbro (powder)+ vitreous carbon trap | 1.5 GPa | $1150^0$ C | 29 Hours | Rich in diopside, phlogopite ± garnet + melt. Rock minerals that have recrystallised include plagioclase and diopside. |
| A-22-080 | Capsule- $Au_{80}Pd_{20}$ Pyroxenite+ gabbro (core)+ vitreous carbon trap | 1.5 GPa | $1150^0$ C | 29 Hours | Plagioclase + Garnet + diopside + enstatite + melt. Rock minerals that have recrystallised include plagioclase and diopside. |

*Table 4.1: Details of experimental run conditions for melt-rock and melt-rock reaction experiments.*

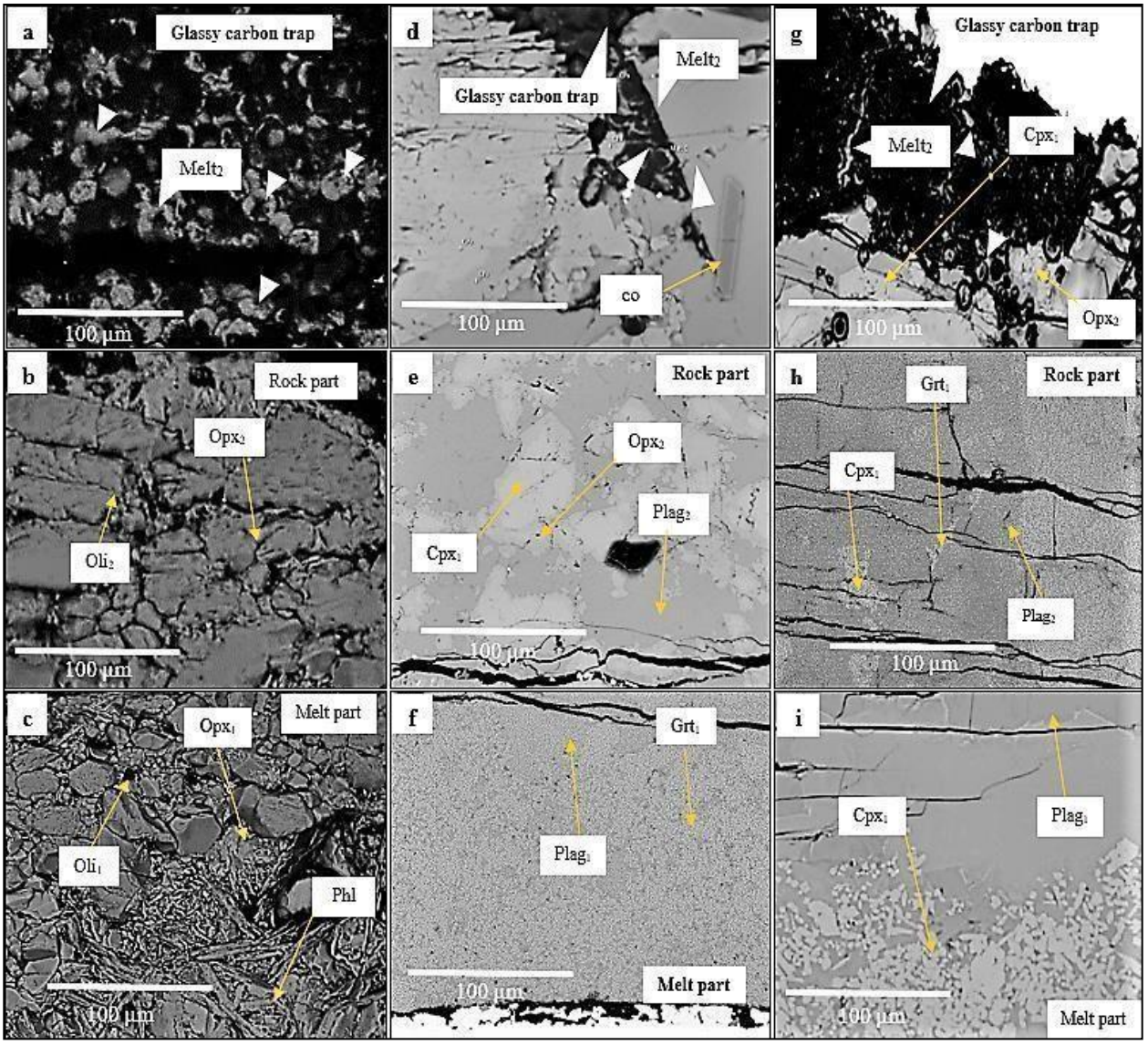


*Figure 4.1: BSE Images of the mineralogical assemblage of melt-rock experimental reactions in $Au_{80}Pd_{20}$ capsule at the pressure of 1.5 GPa and $1200^0$ C for melt-peridotite and $1150^0$ C for melt-gabbro reactions in the mantle wedge and lower crust, respectively. (a) Cross-sectional SEM image of minerals and experimental melts in carbon trap in the peridotite sample, white arrows showing the presence of experimental melts with new compositions within the carbon trap. (b) SEM image of the mineral assemblages in the capsule's middle part (rock part) for the same sample. The sample consists of oli and opx. (c) SEM image of mineralogical assemblages in the capsule's bottom part (melt part). The melt part consists of oli, opx and phl. (d) Cross-sectional SEM image of minerals and experimental melts in carbon trap in the gabbro (powder) sample. White arrows show the occurrence of experimental melt compositions within the carbon trap and the presence of crn mineral grain (e) SEM image of the mineral assemblages in the capsule's middle part (rock part) for the same sample. During the experiments, the melt of phlogopite-pyroxenite reacted with the first-generation cpx grains in the gabbro and produced opx minerals as rims surrounding the cpx core. (f) This is the capsule's bottom (melt) part consisting of cpx, plag and grt minerals. (g) Cross-sectional SEM image of the top part of the capsule with minerals in the gabbro (core) sample. This part comprises a cpx core and a rim of opx minerals. (h) the middle (rock) part of the capsule comprises grt, plag and cpx. (i) Bottom (melt) part of the capsule. This part consists of plag and cpx mineral assembly. Abbreviations or minerals, Phl: phlogopite, Cpx: clinopyroxene, Opx: orthopyroxene, Grt: Garnet, Oli: Olivine, Co: Corrundum. The subscripts in the mineral's abbreviations denote the generation of the mineral, subscript 1: first-generation, 2: second-generation.*

## *4.3. Major oxides chemical analyses*

The major oxide compositions of $Na_2O$, $K_2O$, FeO, MgO, CaO, MnO, $TiO_2$, and $Al_2O_3$ in two different melts produced by reacting the initial melt with both mantle wedge peridotite and the lower crustal gabbro were plotted on bivariate plots against $SiO_2$ (Figure 5.1). The trend of major oxide compositions of the experimentally produced melts has been compared with the chemical composition of some natural volcanic glasses. One of the reasons behind choosing these volcanic arcs is to see how compositionally this melt coincides with the natural volcanic glasses and whether it could describe the origin of rock suits found in the volcanic arcs.

The first-order observation of the bivariate plots (Figure 5.1) shows that in each plot, the phonotephrite melt does not exhibit any compositional similarities with the major oxides composition of volcanic glasses. On the other hand, it is seen that the composition of the shoshonite melt in each plot indicates a chemical relationship with the volcanic glasses.

Calculations of the chemical formula from major oxides analyses on phenocrysts from three representative experimental samples ($SiO_2$ = 44 wt%—55 wt%) are given in Tables 4.3 to 4.7 and reviewed further in the following discussion chapter. All other detailed calculations can be found in the supplementary data – SEM Major Oxides Elemental Analyses (version 1).xlsb.xlsx (sharepoint.com)).

| Oxides | 1 | 2 | 3 | 4 |
|---|---|---|---|---|
| $SiO_2$ | 40.58 | 49.80 | 53.81 | 54.46 |
| $TiO_2$ | 3.51 | 2.76 | 0.22 | 1.20 |
| $Al_2O_3$ | 7.99 | 5.81 | 22.10 | 20.13 |
| FeO | 6.79 | 3.38 | 1.91 | 3.74 |
| MnO | 0.11 | 0.15 | - | 0.13 |
| MgO | 11.72 | 22.53 | 2.71 | 3.05 |
| CaO | 8.64 | 4.31 | 6.14 | 6.66 |
| BaO | 0.53 | - | - | - |
| NiO | - | - | - | - |
| $Cr_2O_3$ | 0.10 | 0.29 | - | - |
| $Sc_2O_3$ | - | - | - | - |
| $Na_2O$ | 1.43 | 0.59 | 4.37 | 4.36 |
| $K_2O$ | 11.30 | 9.03 | 4.14 | 3.10 |
| F | 0.63 | - | - | - |
| $H_2O$ | 5.50 | - | - | - |
| Trace elements | 1.17 | 1.31 | 2.61 | 0.09 |
| Total | 100 | 99.96 | 98.01 | 96.69 |

1. Initial melt, phlogopite-pyroxenite
2. Melt in the melt-peridotite reaction
3. Melt in the melt-gabbro powder reaction
4. Melt in the melt-gabbro core reaction

*Table 4.2: Major oxides compositions of the initial melt and experimentally produced melts after the melt-rock reactions.*

| **Oxides** | **I** | **II** |
|---|---|---|
| $SiO_2$ | 41.12 | 41.52 |
| $TiO_2$ | - | - |
| $Al_2O_3$ | - | - |
| $Cr_2O_3$ | - | 0.14 |
| FeO | 5.99 | 5.81 |
| MnO | 0.21 | 0.20 |
| MgO | 52.61 | 53.18 |
| NiO | 0.30 | 0.28 |
| CaO | 0.08 | - |
| **Sum** | 100.31 | 101.13 |
| *Numbers of ions on the basis of 4 O* | | |
| **Oxides** | **I** | **II** |
| Si | 0.990 | 0.990 |
| Ti | - | - |
| Al | - | - |
| Cr | - | 0.002 |
| Fe (ii) | 0.120 | 0.116 |
| Mn | 0.004 | 0.004 |
| Mg | 1.888 | 1.891 |
| Ni | 0.006 | 0.005 |
| Ca | 0.001 | - |
| **Sum** | 3.009 | 3.009 |

*Table 4.3: Selected olivine analysis calculations from each melt-peridotite reaction experimental sample.*

| Oxides | Gabbro powder | Gabbro core |
|---|---|---|
| $SiO_2$ | 51.42 | 51.85 |
| $TiO_2$ | 0.24 | 0.72 |
| $Al_2O_3$ | 8.94 | 1.63 |
| FeO | 5.27 | 7.90 |
| MnO | 0.14 | 0.22 |
| MgO | 13.65 | 14.59 |
| $Na_2O$ | 1.45 | - |
| CaO | 19.02 | 22.10 |
| **Sum** | 100.14 | 99.02 |
| *Numbers of ions on the basis of 6 O* | | |
| Si | 1.8626 | 1.946 |
| Ti | 0.0065 | 0.020 |
| Al | 0.3816 | 0.072 |
| Fe (ii) | 0.1596 | 0.248 |
| Mn | 0.0043 | 0.008 |
| Mg | 0.7371 | 0.816 |
| Na | 0.1001 | - |
| Ca | 0.7381 | 0.889 |
| **Sum** | 3.9901 | 3.927 |

*Table 4.4: Selected clinopyroxene analysis calculations from each experimental sample.*

| Oxides | Peridotite reaction | Gabbro powder | Gabbro core |
|---|---|---|---|
| $SiO_2$ | 56.55 | 54.18 | 52.99 |
| $TiO_2$ | - | 0.29 | 0.32 |
| $Al_2O_3$ | 2.57 | 0.76 | 0.85 |
| $Cr_2O_3$ | 0.86 | - | - |
| FeO | 4.27 | 18.87 | 18.99 |
| MnO | 0.12 | 0.39 | 0.44 |
| MgO | 35.26 | 24.78 | 24.05 |
| CaO | 0.64 | 1.09 | 1.08 |
| **Sum** | 100.27 | 100.36 | 98.72 |
| *Numbers of ions on the basis of 6 O* | | | |
| Si | 1.933 | 1.978 | 1.972 |
| Ti | - | 0.008 | 0.009 |
| Al | 0.067 | 0.022 | 0.025 |
| Al | 0.037 | 0.011 | 0.012 |
| Cr | 0.023 | - | - |
| $Fe^{3+}$ | 0.009 | 0.033 | 0.037 |
| $Fe^{2+}$ | 0113 | 0.543 | 0.554 |
| Mn | 0.004 | 0.012 | 0.014 |
| Mg | 1.797 | 1.349 | 1.334 |
| Ca | 0.023 | 0.043 | 0.043 |
| **Sum** | 4.007 | 3.998 | 4.000 |

*Table 4.5: Selected orthopyroxene analysis calculations from each experimental sample.*

| Oxides | I | II |
|---|---|---|
| **$SiO_2$** | 44.12 | 51.97 |
| **$TiO_2$** | 2.56 | 2.51 |
| **$Al_2O_3$** | 11.72 | 6.61 |
| **$Cr_2O_3$** | 0.98 | 0.33 |
| **FeO** | 1.88 | 2.80 |
| **MgO** | 26.76 | 26.18 |
| **CaO** | - | 1.52 |
| **$Na_2O$** | - | 0.79 |
| **$K_2O$** | 10.42 | 8.92 |
| **Sum** | 98.44 | 101.30 |
| *Numbers of ions on the basis of 22 O* | | |
| **Oxides** | **I** | **II** |
| **Si** | 5.989 | 6.755 |
| **Ti** | 0.261 | 0.245 |
| **Al** | 1.875 | 1.013 |
| **Al** | 0.000 | 0.000 |
| **Cr** | 0.021 | 0.034 |
| **$Fe^{2+}$** | 0.213 | 0.304 |
| **Mg** | 5.415 | 5.073 |
| **Ca** | - | 0.094 |
| **Na** | - | 0.003 |
| **K** | 1.804 | 1.479 |
| **Sum** | 15.578 | 15.001 |

*Table 4.6: Selected phlogopite analysis calculations from melt-peridotite reaction sample.*

| Oxides | Gabbro powder | Gabbro core |
|---|---|---|
| **$SiO_2$** | 44.88 | 41.04 |
| **$TiO_2$** | 0.19 | 0.62 |
| **$Al_2O_3$** | 24.89 | 22.28 |
| **FeO** | 9.10 | 11.24 |
| **MnO** | 0.27 | 0.67 |
| **MgO** | 17.15 | 15.50 |
| **CaO** | 4.63 | 8.68 |
| **Sum** | 101.11 | 100.03 |
| *Numbers of ions on the basis of 22 O* | | |
| **Oxides** | **Gabbro powder** | **Gabbro core** |
| **Si** | 6.251 | 5.978 |
| **Al** | 4.086 | 0.022 |
| **Al** | | 3.803 |
| **Ti** | 0.020 | 0.068 |
| **FeO** | 1.060 | 1.369 |
| **MgO** | 3.561 | 3.366 |
| **MnO** | 0.017 | 0.083 |
| **Cao** | 0.691 | 1.354 |
| **Sum** | 15.686 | 16.042 |

*Table 4.7: Selected garnet mineral analysis calculations from each experimental sample.*

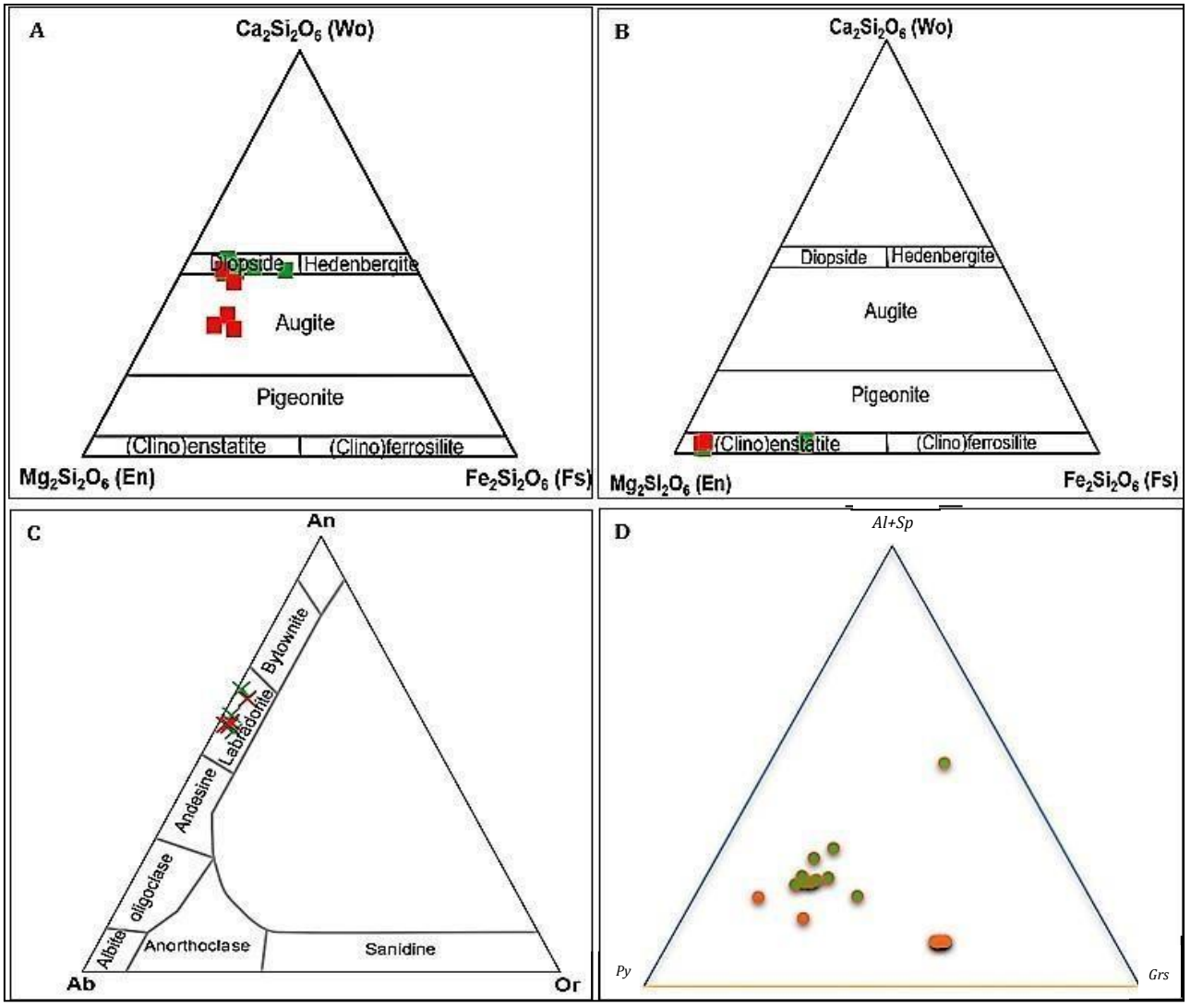


*Figure 4.2: (A) Clinopyroxene triangular plots in gabbro powder (Green squares) and gabbro core (Red squares) reaction experiment. The end-members in this ternary diagram are Wo = Wollastonite, En = Enstatite & Fs = Ferrosilite, (B) Orthopyroxenes plots in pyroxene triangular diagram in the melt-peridotite (Green Squares) and melt-gabbro (Red squares) reactions, (C) Reaction of starting melt with gabbro (both powder and core) producing plagioclase in the lower crust, essential labradorite in compositions. Red crosses represent labradorite plagioclases formed in the gabbro powder samples, and the green crosses denote plagioclases from the gabbro core sample. The end-members in this ternary diagram are Ab = Albite, Or = Orthoclase & An = Anorthotite, (D) Garnet compositions in melt-gabbro powder sample (Green circles) and melt-gabbro core sample (Red circles) reactions. The end-members on each vertex are Al+Sp = Almandine + Spessartine garnet, Py = Pyrope garnet & Grs = Grossular garnet.*

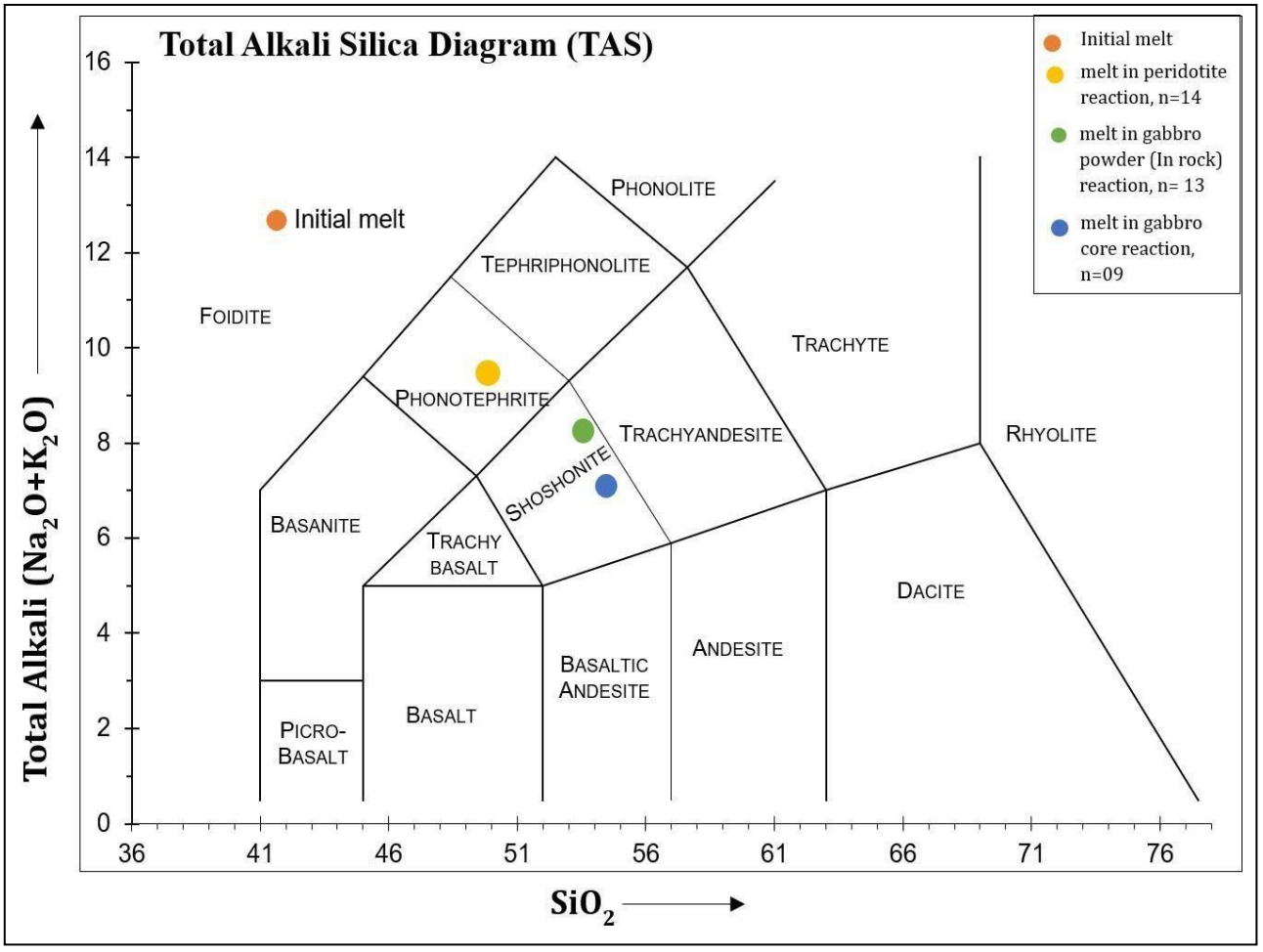


*Figure 4.3: Total Alkali-Silica (TAS) diagram for magma series after Le Bas et al., 1986. The 'RED' solid circle in the foidite field in the TAS diagram represents the initial homogeneous partial melt of phlogopite-pyroxenite. The 'Orange' solid circle represents the experimentally produced phonotephrite melt in the peridotite sample (M-22-054) during the reaction of the initial melt with mantle wedge peridotite melt-peridotite reaction. The 'Green' & 'Dark Blue' solid circles representing melts of shoshonitic compositions were produced experimentally during the reaction of the initial melt with gabbro powder (A-22-079) and gabbro core (A-22-080). The upper right box is the legend, and 'n' is the number of data points averaged to get to each coloured point on the graph.*

.

## *4.4 Trace elemental analyses*

Before conducting the reaction experiments, a crucial step was to dope the initial melt with twenty-one trace elements, including lithophile elements like Rb, Cs, Ba and $Eu^{2+}$, and also the light & heavy REEs with high concentrations (Table 4.8). Due to high-pressure melt-rock reactions, the concentrations of trace elements in the experimentally produced melts are significant to the starting partial melt from hydrous pyroxenite.

Figure 4.5 illustrates Ba concentration plots showing the variations in Ba concentration in the shoshonitic melt within the carbon trap for the melt-gabbro powder sample (Sample ID: A-22-079). As the depth of the melt increases transversely within the capsule, the concentration of Ba in the melt increases with the time of spot analysis. It is interesting to note that there is a sudden drop in the Ba concentration in the analysis. This sudden decline in Ba could be due to the laser beam analysis intersecting more carbon beads relative to melt in the carbon trap. Since the carbon beads do not contain Ba within them, fluctuation in the Ba concentrations can be used as a proxy for the proportion of melt and carbon beads in each time slice of the laser ablation signal.

Figure 4.6a represents the bivariate plot for Ba/La, which has a positive slope in the plot. This line comprises two ending members; the carbon trap is placed in the lower left corner, and the experimental melt is placed in the upper right corner of the line. Based on the bivariate plot, it can be seen that the melt has a high Ba/La ratio, which is indicative of the melt. On the other hand, figure 4.6b illustrates a different bivariate plot with Ba and Co as the variables. Based on the slope of this plot, the carbon beads in the melt trap may contain a significant amount of cobalt, which is why there is a negative slope on the plot. Consequently, during the laser ablation analysis, cobalt marked a high signal; this was evident by the high enrichment for cobalt in the experimental melts.

Figure 4.7 compares enrichment and depletion factors between phonotephrite melt and shoshonite melt produced during melt-rock reactions. In phonotephrite melt, there are a few LILEs that are enriched, whereas the REEs are strongly depleted (Figure 4.7a). Conversely, shoshonite melt is strongly enriched in some LILE elements (Figure 4.7b), while some heavy rare earth elements (HREEs) are slightly depleted. It is interesting to note that both phonotephrite and shoshonite melts are enriched in Hf and are significantly depleted in U and Th; this is contrary to the behaviour of these three elements in most island arcs, in which Hf

behaves similarly to U and Th.

| Elements | Concentrations in the mixture |
|---|---|
| B | 1000 |
| Cu | 500 |
| S | 500 |
| Nb | 1000 |
| Ce | 500 |
| Eu | 500 |
| Th | 500 |
| Dy | 500 |
| Er | 500 |
| Hf | 500 |
| Ho | 500 |
| Ho | 500 |
| La | 700 |
| Rb | 500 |
| U | 500 |
| Yb | 500 |
| Ba | 500 |
| Co | 500 |
| Lu | 500 |
| Y | 500 |
| Cs | 500 |
| Nd | 500 |
| **Sum** | 11700 |

*Table 4.8: Trace elemental (in ppm) concentrations added to the initial melt.*

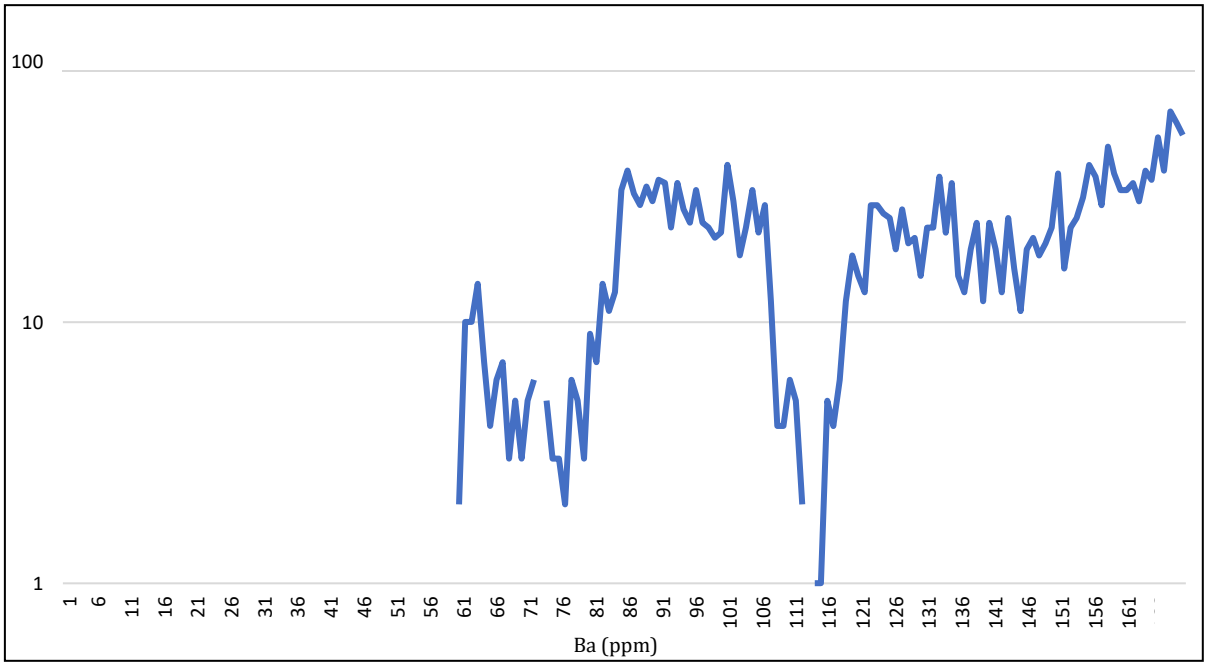


*Figure 4.5: $Ba^{138}$ plots on a logarithm scale with factor 10. This plot shows the variations in Ba concentration in the shoshonitic melt within the carbon trap for the gabbro sample.*

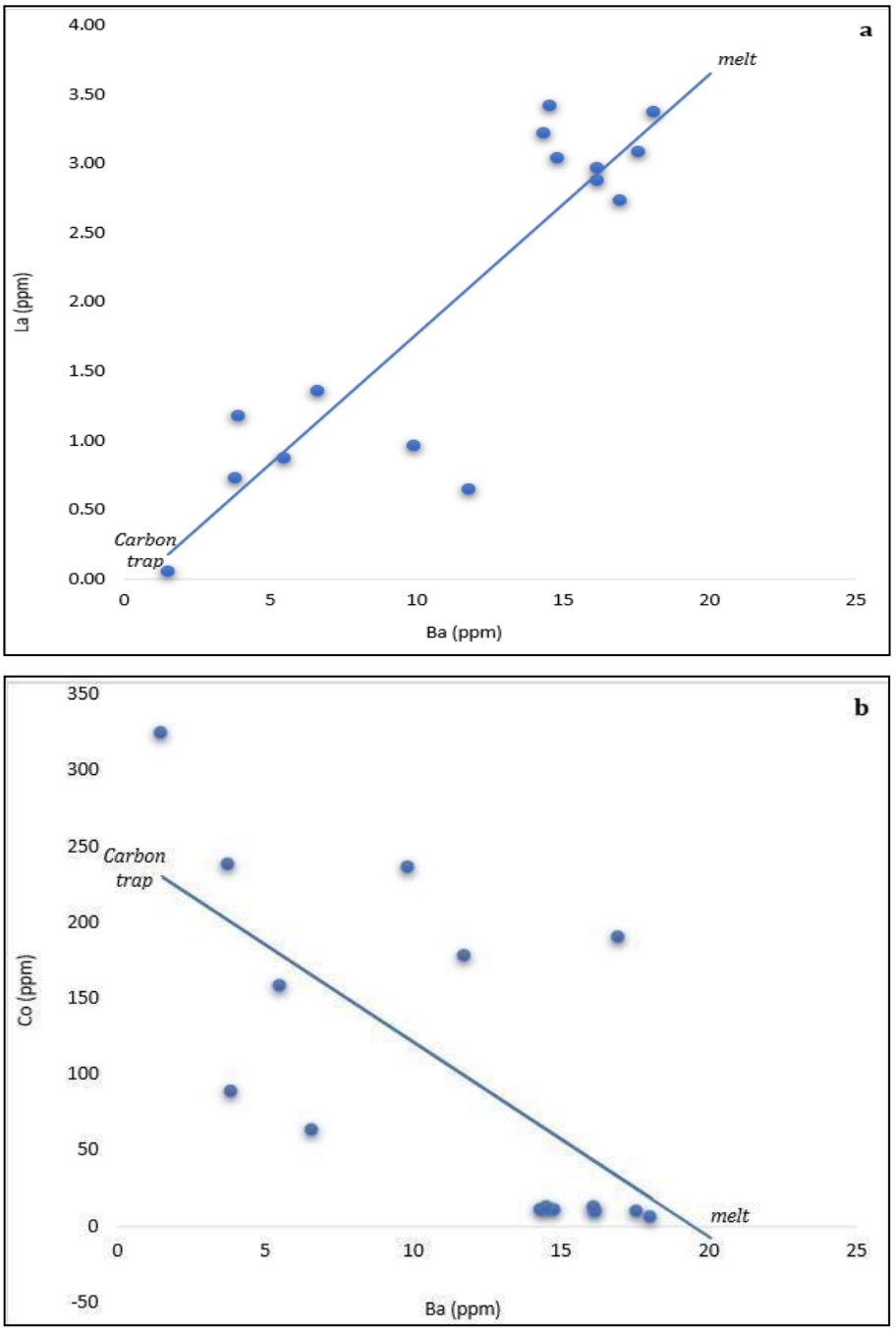


*Figure 4.6: $Ba^{138}$ vs $La^{139}$ and $Ba^{138}$ vs $Co^{59}$ bivariate plots for shoshonite melt produced during the reaction between initial melt with the gabbro powder sample. (a) this bivariate plot has a positive slope in the plot. On the slop, there are two end-member, the carbon trap is placed on the lower left corner, and the experimental melt lies on the upper right corner of the line. This plot suggests that the shoshonite melt gives a high ratio of the Ba/La. (b) The plot shows a negative slope on the graph, which is opposite to the previous plot of Ba/La. This slope indicates that the carbon trap contains a considerable amount of cobalt compared to the experimental melt. That is why cobalt gives a high content during analysis.*

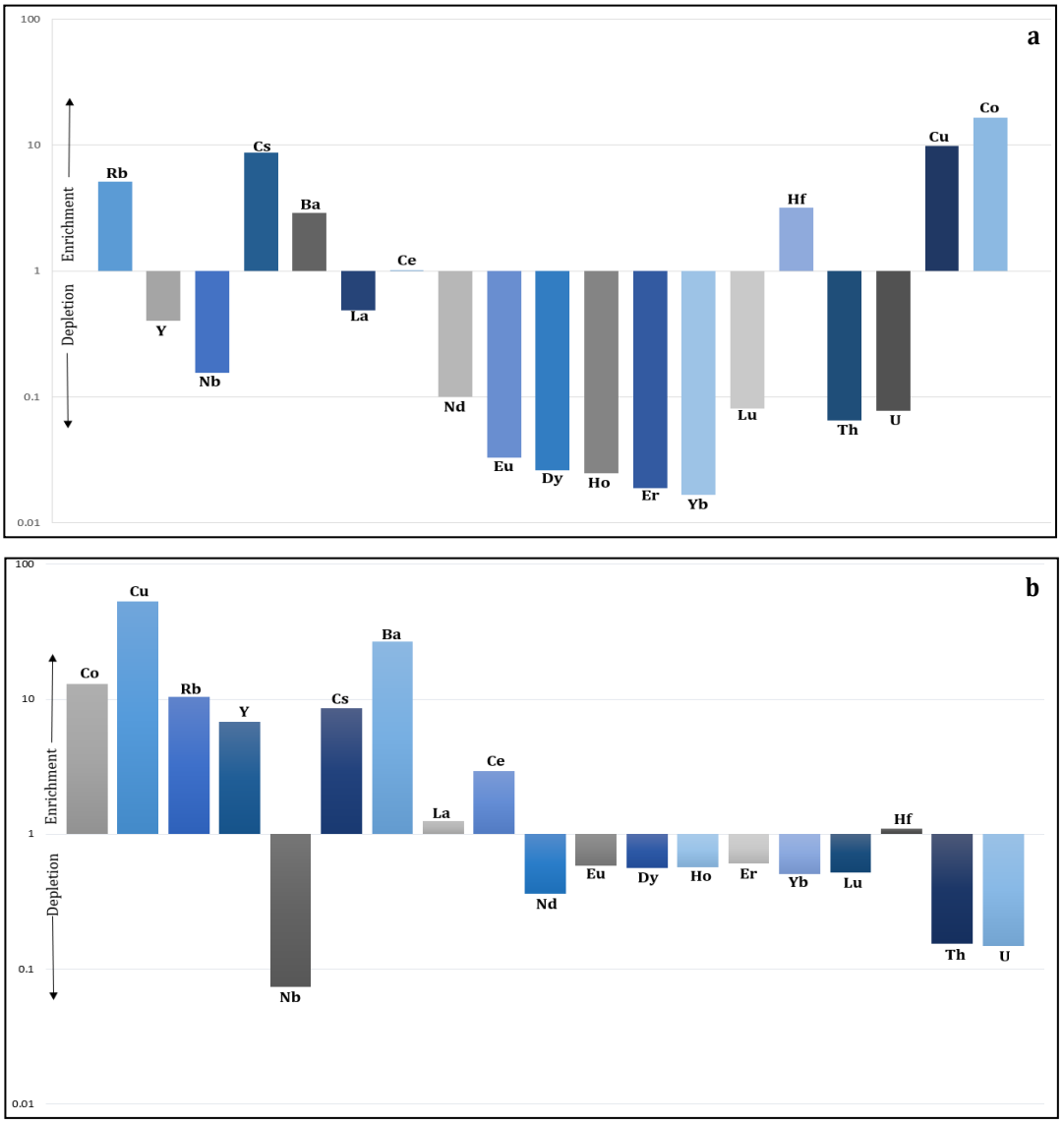


*Figure 4.7: Enrichment- Depletion diagrams showing the enrichment factor for 21 trace elements in experimentally produced melts. (a) Represents the enrichments of Rb, Cs, Ba, Ce, Hf, Cu and Co elements in experimentally produced phonotephrite melt in melt-peridotite reaction sample, (b) showing the enrichment of CO, Cu, Rb, Y, Cs, Ba, La, Ce and Hf in experimentally produced shoshonite melt in the melt-gabbro reaction sample.*

# Chapter 5: Discussion

## *5.1. Understanding the key sub-arc melt-rock reactions*

### *5.1.1. Melt-rock reactions in the mantle wedge*

The time-series experiments had more starting melt proportions than the peridotite and a small proportion of carbon traps. The reaction experiments showed that the partial melt of phlogopite-pyroxenite reacted with peridotite and modified the initial melt to phonotephritic composition. The key melt-rock reaction in the mantle wedge is determined to be $Ol_1 + Opx_1 + melt_1 = Ol_2 + Opx_2 + Phl + melt_2$.

### *5.1.2. Melt-rock reactions in the lower crust*

In two different melt-rock reaction experiments, the melt-rock experiments had more starting melt proportions than dry gabbro powder and gabbro core and a small proportion of carbon traps. In both melt-rock reaction experiments, the reactions with the initial melt, the key melt-rock reaction in the lower crust are defined as $Opx_1 + Cpx_1 + Plag_1 + Melt_1 = Opx_2 + Cpx_1 + Plag_2 + Grt_1 + Melt_2$.

## *5.2. Determining the changes in melt composition during melt-rock reactions*

### *5.2.1. Reaction between the mantle wedge peridotite and melt*

The reaction of the initial melt with the mantle wedge peridotite resulted in the formation of a melt of new composition. This reaction led to a significant increase in the percentage of $SiO_2$ to 49.89 wt% in the experimentally produced melt compared to the initial melt. As compared to the initial melt, the new melt contains a higher percentage of MgO, MnO, and $Cr_2O_3$ and a lower percentage of $TiO_2$, $Al_2O_3$, FeO, $Na_2O$, and $K_2O$. Olivine, on the other hand, exhibits an average magnesium number of 89.57 after chemical reactions. Furthermore, among all trace elements, the heavy rare earth elements (HREEs) are strongly depleted in this melt and have the highest enrichment in Co, Cu and Cs (Figure 4.7a).

### *5.2.2. Reaction between the lower crustal gabbro and melt*

As a result of the reaction between the lower crustal gabbro and the initial melt, the percentage of silica in the experimentally produced new melt increased significantly ($SiO_2$ >52 wt%). Comparing the new melt with the initial melt, the $TiO_2$, MnO, MgO, and CaO

contents in the new melt decreased, and $Al_2O_3$, $Na_2O$, and $K_2O$ contents increased (Table 4.2, columns 3 & 4). Moreover, the chemical analysis shows that heavy rare earth elements (HREEs) in this melt are slightly depleted and enriched in Co, Cu and Ba (Figure 4.7b) in comparison to the original melt.

## *5.3. Comparison between the compositions of experimental volcanic glass (melt) and natural volcanic arc glasses*

The lower crustal melt-rock reactions altered the composition of the initial melt to shoshonite (Figure 4.3) with an increased concentration of silicon, aluminium, and alkali oxides and a reduction in iron and magnesium oxides. Contrariwise, The melt-rock reactions in the mantle wedge on the other hand changed the composition of the starting melt to phonotephrite composition (Figure 4.3), with higher concentrations of silicon oxide, manganese oxide, and magnesium oxide and lower concentrations of aluminium, calcium, iron, and alkali oxides. One of the main reasons to choose some published data for comparison is to check whether the starting material with which we started our reactions could explain the formation of the rock suits found in volcanic arcs.

In relation to experimentally produced phonotephrite melt, the ankaramitic absarokite flows in Carmacks group in Yellowstone have MgO ranges up to 15 wt% and contains olivine phenocrysts with Mg compositions as high as $Fo_{93}$. Besides, the results of the melt-peridotite reaction show that the phonotephritic melt consists of an average amount of 18.53 wt% MgO. At the same time, the olivine phenocrysts in the melt-peridotite sample are compositionally similar to Carmacks absarokites (phonotephrite melt has Mg-rich olivine of $Fo_{93.6}$). Besides, the experimentally generated phonotephritic melt suggests the presence of high concentrations of total alkali (>9 wt%) and moderate concentrations of $SiO_2$ (44 – 51 wt%) and a very low amount of $Al_2O_3$ (4.45 – 6.61 wt%). Furthermore, this phonotephrite melt has an average high Ca/Al ratio of 0.823, which is reasonably similar to some Carmacks group absarokite lava, which has low Ca contents in combination with a high Ca/Al ratio. Combined with the major oxide chemistry, the experimentally produced phonotephritic melt exhibits a periodic variation in LILE elements such as Rb/Ba (0.402-0.140) and K/Na (3.607 – 22.878) (Figure 4.7a). It is similar to the absarokite lavas of the Carmack group, which show systematic variation in the LILE proportions (e.g., Rb/Ba, K/Na).

Most of the Fiji volcanics show a high trend in MgO (>8.3 wt% MgO) absarokite composition. In contrast, the MgO content of phonotephrite melt is very high (with an

average of ~18.53 wt% MgO). On the other hand, shoshonite melts in the melt-gabbro reaction experiments contain more CaO (>5.8 wt% CaO) and less MgO (average ~2.88 wt% MgO), and the $K_2O/Na2O$ ratio varies between 0.94 – 1.4 with >3.1 wt% $K_2O$ at $SiO_2$ >50%, which chemically resembles the Viti Levu, Fiji shoshonites.

Most of the rocks found in the Zedong terrain in southern Tibet are absarokites in composition, with $SiO_2$ content between 45 wt% to 52 wt% with the increasing content of $K_2O$. Some are more evolved into shoshonite and banakite rocks. Aside from $K_2O$, the absarokites have similar concentrations of the major elements. Compared to. The ocean. Island basalts, which are found in island arcs and tend to have higher concentrations of minor elements. The phonotephritic melt which has been produced during the reaction between the initial meltand peridotite (e.g., sample M-22-054, Figure 4.1a–c) show a high concentration of total alkali (>9 wt%) and moderate concentrations of $SiO_2$ (44 wt%– 51 wt%). The major oxides chemical analyses of the experimentally produced shoshonitic melts in gabbro samples (e.g., sample A- 22-079 & A-22-080, figure 4.1d & 4.1g) indicate that the melts contain 3.10 wt% to 4.14 wt% of $K_2O$, and the $K_2O/Na_2O$ ratios for these melts range between 0.94 and 0.71. However, shoshonite melts have high levels of $SiO_2$ (52 wt% – 55 wt%), tend to have a high amount of total alkalis ranging between 7 wt% – 8 wt% (Figure 4.3), and high aluminium oxide percentages (19.30 wt% to 22.10 wt%).

The reactions between the initial melt and gabbro show that the composition of the shoshonite melt is comparable to the natural volcanic glass compositions from a few volcanic arcs, which are rich in $K_2O$. The shoshonites from the western Kunlun orogenic belt have high $K_2O$ content (2.54 wt% – 10.95 wt%, average 5.48 wt%), and high $K_2O/Na_2O$ ratios (>0.6 for $SiO_2$ <55 wt% and >1 for $SiO_2$ >55 wt%). Moreover, these rocks also have high but variable $Al_2O_3$ content (13.11 wt%–19.20 wt%), high $Fe_2O_3/FeO$ ratio (0.85–1.51, with an average of wt%) and a low $TiO_2$ content (0.15 wt% – 1.12 wt%, with an average of 0.57 wt%). These chemical signatures are similar to the experimentally produced shoshonite melts, which evolved during the reactions between the initial melt and lower crustal gabbro. This experimentally generated shoshonites have $K_2O$ ranges from 2.55 wt%– 4.42 wt%, the average is 3.95 wt%, and high $K_2O/Na_2O$ ratios of 0.94 – 0.71 for $SiO_2$ <55 wt%. The content of $Al_2O_3$ is also high and varies between 18.11 wt% and 22.10 wt% and has an almost similar high ratio of $Fe_2O_3/FeO$ (0.70 – 1.91) and low $TiO_2$ content range between 0.22 to 1.20 wt% as western Kunlun orogenic belt shoshonites. According to the chemical analysis of major oxides, all samples of western Kunlun shoshonitic plutons are potassium-rich and are predominantly lying within the shoshonite field as described by Peccerillo & Talyor 1976; further, $SiO_2$ generally ranges between 45 wt% to 75 wt% at high $K_2O$ (typically >3.5%). In spite of their high

content of $K_2O$, they are Not considered as ultra-potassic, maintaining a $K_2O/Na_2O$ ratio between 0.5 and 2.0, likewise thin the Shoshonitic magma field. Additionally, post-collisional shoshonites from the Tibetan plateau display a variable Mg number [=MgO/ (MgO x 0.8 + $FeO_{Total}$)] from 73 to 10, with increasing values of $SiO_2$ and $Al_2O_3$. At the same time, $Fe_2O_3$ and CaO (which have an inflexion at 5% MgO declined The decrease in magnesium oxide. Compared to these post-collisional Tibetan shoshonites, experimentally produced shoshonites show very similar chemical characteristics in terms of Mg number ranging between 73 to 44, with rising Si and Al oxide percentages and a decreasing amount of iron and calcium oxides with MgO. The experimentally produced shoshonites show very high enrichment of Rb, Cs, Ba, Ce, Hf, Cu & Co elements and depletion in Y, Nb, La, Nd, Dy, Eu, Ho, Er, Lu, Yb. It is also important to note that Hf shows the opposite trend to Th and U. While Hf is slightly enriched in the melt; on the other hand, U and Th are sharply depleted in the shoshonite melt. This result opposes the chemical characteristics of island arc magma, where these three elements behave similarly.

Furthermore, in the Tibetan plateau shoshonite, there is an inflected trend of $TiO_2$, with average excesses of 13 wt% to 15 wt% for $A1_2O_3$ and 0 wt% to 5 wt% for $TiO_2$, respectively, and low absolute abundances of $TiO_2$ and $A1_2O_3$. Likewise, $Na_2O$ and $K_2O$ have relatively continual surpluses, though $K_2O$ is always slightly higher than the $Na_2O$ ($Na_2O/K_2O$ <2). In contrast to the Tibetan plateau shoshonites, the experimentally produced shoshonites have slightly lower $K_2O$ than $Na_2O$ content, with a $K_2O/Na_2O$ ratio ranging between 0.94 and 0.71 (Table 4.2). Several other chemical signatures also intensify the idea that the experimentally generated shoshonite melt is chemically similar to the western Kunlun shoshonites and post-collisional Tibetan shoshonites. In addition to the Tibetan plateau shoshonite, experimentally produced shoshonite melt contains certain LILE elements and incompatible elements similar to the Tibetan plateau shoshonite. It is notable that La has a moderate but variable content in the melt, while Eu shows a predominantly negative anomaly (Figure 4.7b). Further, the melt also has a high degree of variation in the ratios; for example, the percentage of Ba/La varies from 2.297 to 42.424, that of La/Yb varies between 1.967 and 23.243, and that of La/Nb varies between 3.14 and 71.379.

Additionally, in the Lavras do Sul shoshonitic association in southernmost Brazil, the basic volcanic rocks have higher values of $K_2O$ than $Na_2O$, which are categorised as shoshonites and potassic trachybasalts (Le Maitre, 1989). They are generally composed of nearly saturated silica with normative olivine (9.75–23.25), hypersthene (8.19), and diopside (3.71–18.70). The aluminium content ranges from 11.43 wt% to 14.50 wt%, whereas the experimentally

produced shoshonite melt is slightly rich in aluminium (averagely~21.16 wt%); the lesser values are attributed to the accumulation of olivine and clinopyroxenes as indicated by the simultaneous rise in magnesium content from 8.20 wt% to
13.00 wt%. Gest and McBimey (1979) have suggested that is shoshonites are obtained from more basic magmas through the fractionation of olivine and pyroxene.

An important observation from the bivariate plot for $SiO_2$ vs $Al_2O_3$ (Figure 5.1) is that the phonotephrite melt produced during the melt-peridotite reaction has a low aluminium content compared to shoshonite melt in gabbro. This is because gabbro is largely composed of plagioclase and clinopyroxene, whereas the plagioclase feldspar has a high percentage of aluminium. As a result, at the higher-pressure melt-rock reactions (>9 Kbar pressure) in the mid to lower crustal depth, a plagioclase breakdown reaction occurred in which calcic plagioclase breaks down to form corrundum (Figure 4.1d) and a melt with high aluminium content (Wood, 1978).

All the regions of the island arcs that have been studied for the presence of shoshonites (e.g., New Guinea, Indonesia, Kamchatka, and Fiji) represent the latest volcanic events. This is because they are located the farthest from the trenches. As far as their mineralogy is concerned, they are similar to the alkali basalts of Japan and the Aleutians. However, they differ principally in their K/Na relationships and corresponding lithology. Similarly, an increase in potassium concentration in the western Aleutians was reported, with a transition from submarine assemblages to subaerial Assemblages and a decline in the enrichment of iron (Wilcox, 1959). Interestingly, out of all the areas investigated, only the Viti Levu the volcanic centre has a clear secular evolution from the tholeiitic to calc-alkaline and then to shoshonitic volcanism.

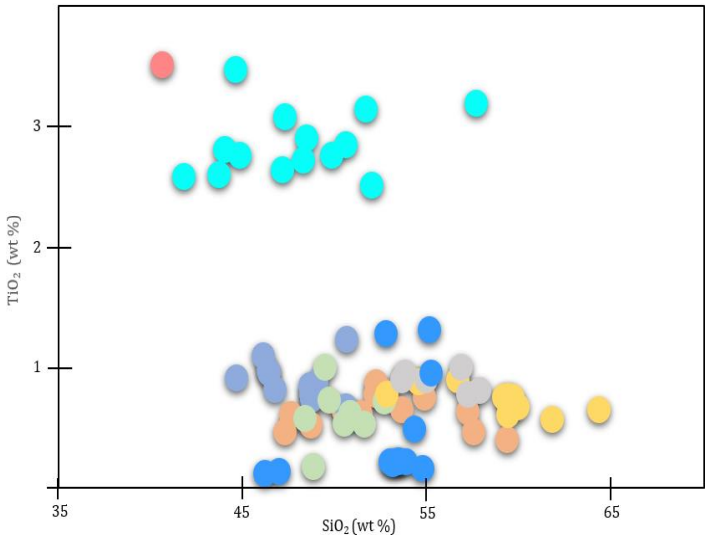
3
2
1
TiO2 (wt %)
35
45
55
65
SiO2 (wt %)

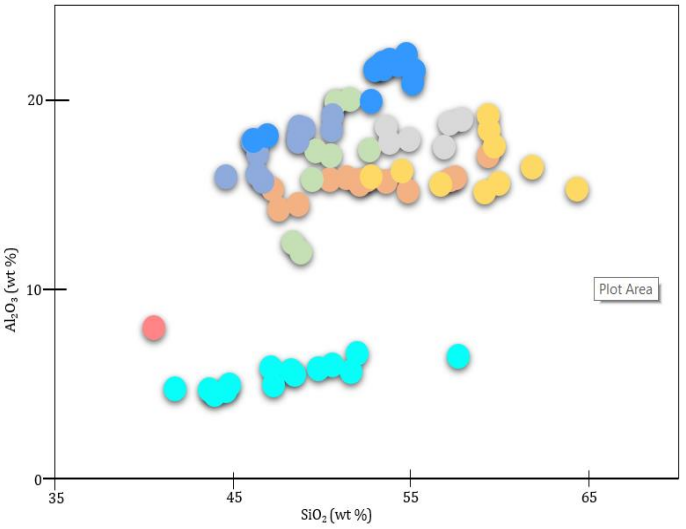
20
10
0
Al2O3 (wt %)
Plot Area
35
45
55
65
SiO2 (wt %)

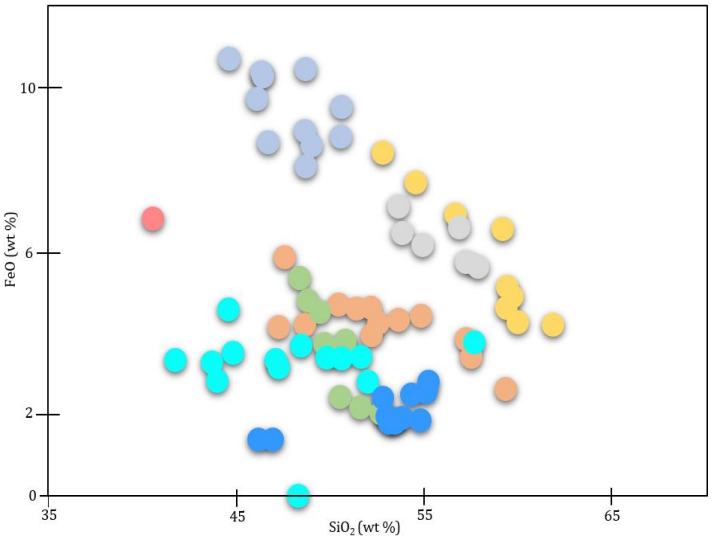
10
6
2
0
FeO (wt %)
35
45
55
65
SiO2 (wt %)

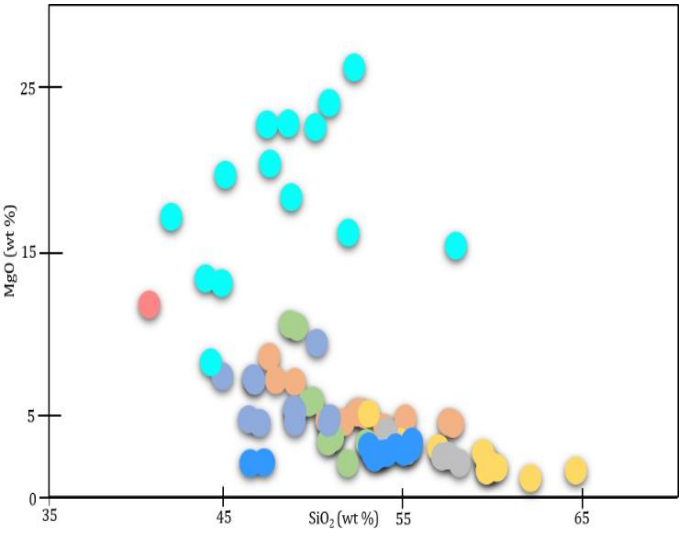
25
15
5
0
MgO (wt %)
35
45
SiO2 (wt %)
55
65

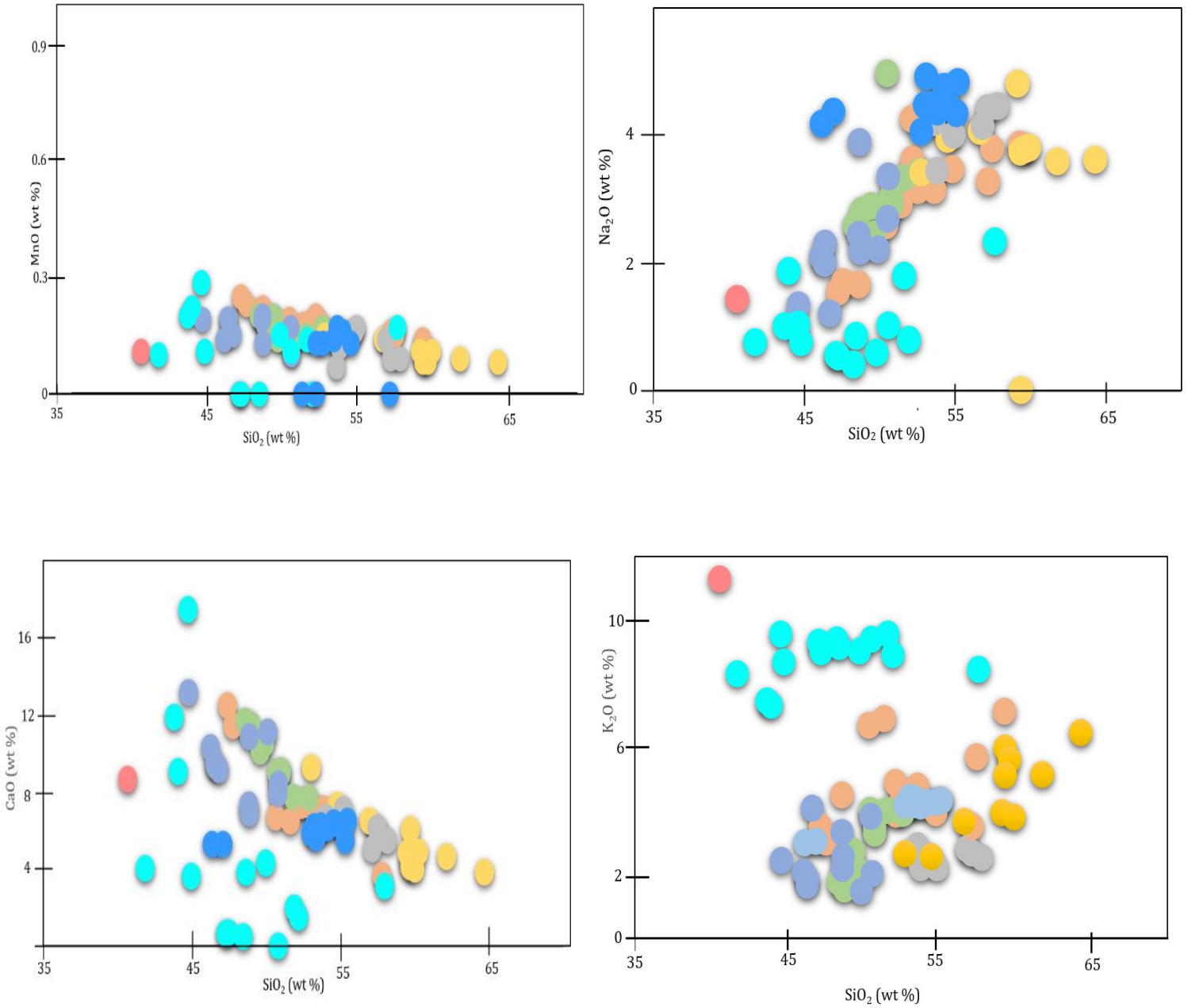


*Figure 5.1: Major oxides compositional bivariate comparison plots between the experimentally produced melts and natural volcanic glass compositions from a few volcanic arcs. Orange circle: Kamchatka arc; Green circles: Viti Levu, Fiji; Yellow circles: Kunlun Belt; Blue circles: Southern Tibet; Light grey circles: Southernmost Brazil; Light blue circle: Melt in Peridotite; Dark blue circles: Melt in Gabbro Powder; Red solid circle: Initial melt composition.*

# Chapter 6: Conclusion

The melt-rock reaction experimental study was focused on the volcanic arcs in subduction zone settings. The study began with a homogeneous partial melt of phlogopite-pyroxenite reacting with peridotite of the mantle wedge and lower crustal gabbro. This study explored the following questions (1) how does chemistry changes along sub-arc melt migration pathways during melt-rock reactions, (2) what are the main sub-arc melt-rock reactions that take place during melt ascent through mantle wedge and lower crust, and (3) could this melt explain the origin of the rock suites found in arc settings? In addition to these questions, the study has also explored the frequency of occurrence of this melt beneath the global volcanic arcs.

Interestingly, the major and trace elemental data obtained from phonotephrite melt does not clearly indicate any chemical relationships with the other natural volcanic arc settings. The bivariate plots of the major oxides (Figure 5.1) suggest that the chemical compositions of phonotephrite melt appear quite distant from other natural volcanic glass compositions, on the other hand, is more inconsistent with the rocks found in volcanic arc settings. Conversely, the shoshonite melts, on the other hand, show a similar geochemical trend to the other natural volcanic arc settings. Consequently, two possible explanations could be as follows:

(1) First, the initial melt used in the reaction experiments is uncommon beneath volcanic arc crust and found only in a few volcanic arc settings globally but is rather more common in intraplate volcanic settings (Figure 6.1).

(2) Second, since the occurrence of the initial melt is rare beneath the arc crust, reactions of harzburgite peridotite with this melt in the mantle wedge are also occasional in subduction zone settings. For this reason, it cannot explain the magma generation processes in subduction zone settings.

Taking into account the most recent studies and interpretations of the hybridisation of melt with the mantle and lower crust, some future melt-rock experimental studies at much higher pressure (from 4 to 4.5 GPa pressure, ~depth 120 – 135 km) and $1250^0$ C temperature would enrich our current understanding through conducting repeated melt-rock reactions and comprehending how mantle hybridisation processes contribute to subduction zone magmatism. In future studies, we will conduct a series of reactions in three distinct ways. 1) In the first part, we will conduct a series of reactions between the mantle wedge peridotite and mica-pyroxenite partial melts at a pressure of 4 – 4.5 GPa and $1250^0$ C temperature, 2) this

would be followed by reacting the new resulting melt from the first experiment with lower crustal gabbro, and 3) a different approach could be to mix the melt and rock components of the experiment so that there will be no separate layers of melt and rock powder in the capsule. Besides these crucial steps in reaction experiments. In addition, a further required piece of future work is to characterise the carbon beads better so that we know which trace elements are affected by the ablation of beads and the glass in the melt traps. As a result of these repeat reaction studies, we will be able to assess the melt-rock reaction studies in two ways: 1) understanding melt equilibration via the series of melt-rock reactions and 2) enriching our current interpretation of the fractionation trend of absarokite-shoshonite-banakite magma.

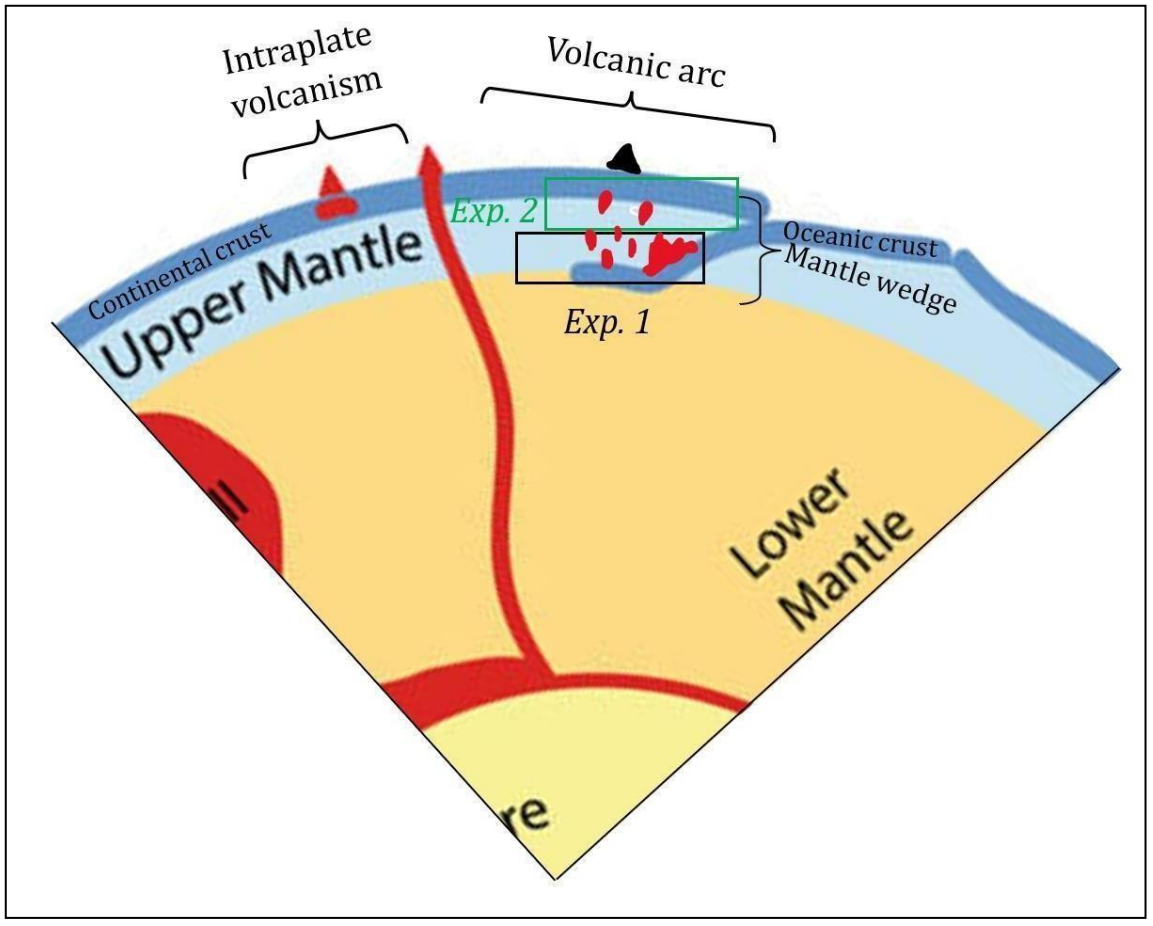


*Figure 6.1: An example of a schematic cross-sectional diagram of a subduction zone and intraplate volcanic setting. The phlogopite-pyroxenite melt (initial met) occurs (represented by red-coloured droplets) above the subducting oceanic crust beneath overriding continental lithosphere, which migrates upward into the mantle wedge where it reacts with harzburgite peridotite; the 'Black square' box shows the location of these reactions. The melt progressed further up and reacted with the lower crustal gabbro, represented by the 'Green square' on the diagram.*

# Supplementary Data

The links below contain the additional supplementary data set:

Supplementary Data - OneDrive (sharepoint.com)

ImageMatrix

https://imagematrix.science.mq.edu.au/viewer/?mode=view&id=849

https://imagematrix.science.mq.edu.au/viewer/?mode=view&id=859

https://imagematrix.science.mq.edu.au/viewer/?mode=view&id=850

FEI SEM BSE Images

FEI BSE Images - OneDrive (sharepoint.com)

SEM major oxides elemental analyses
SEM Major Oxides Elemental Analyses (version 1).xlsb.xlsx (sharepoint.com)

La-ICP-MS traceelementalanalyses
Run1_TRANSPOSED.csv (sharepoint.com)

Run2_TRANSPOSED.csv (sharepoint.com)

# References


Aldanmaz, E. R. C. A. N., Pearce, J. A., Thirlwall, M. F., & Mitchell, J. G. (2000). Petrogenetic evolution of late Cenozoic, post-collision volcanism in western Anatolia, Turkey. *Journal of volcanology and geothermal research*, *102*(1-2), 67–95.

Allègre, C. J. (1982). Chemical geodynamics. *Tectonophysics*, *81*(3-4), 109-132.

Arculus, R. J. (1994). Aspects of magma genesis in arcs. *Lithos*, *33*(1-3), 189-208.

Arculus, R. J., & Johnson, R. W. (1978). Criticism of generalised models for the magmatic evolution of arc-trench systems. *Earth and Planetary Science Letters*, *39*(1), 118-126.

Atherton, M. P., & Tarney, J. (Eds.). (1979). *Origin of Granite Batholiths: Geochemical Evidence: Based on a Meeting of the Geochemistry Group of the Mineralogical Society*. Shiva Pub. Limited.

Ayati, F., Yavuz, F., Asadi, H. H., Richards, J. P., & Jourdan, F. (2013). Petrology and geochemistry of calc-alkaline volcanic and subvolcanic rocks, Dalli porphyry copper-gold deposit, Markazi Province, Iran. *International Geology Review*, *55*(2), 158-184.

Baker, D. R., & Eggler, D. H. (1987). Compositions of anhydrous and hydrous melts coexisting with plagioclase, augite, and olivine or low-Ca pyroxene from 1 atm to 8 kbar; application to the Aleutian volcanic centre of Atka. *American Mineralogist*, *72*(1-2), pp. 12–28.

Borg, L. E., Clynne, M. A., & Bullen, T. D. (1997). The variable role of slab-derived fluids in the generation of a suite of primitive calc-alkaline lavas from the southernmost Cascades, California. *The Canadian Mineralogist*, *35*(2), 425–452.

Borghini, G., Rampone, E., Zanetti, A., Class, C., Cipriani, A., Hofmann, A. W., & Goldstein, S. L. (2016). Pyroxenite layers in the Northern Apennines' upper mantle (Italy)—generation by pyroxenite melting and melt infiltration. *Journal of Petrology*, *57*(4), 625–653.

Brenan, J. M., Shaw, H. F., Phinney, D. L., & Ryerson, F. J. (1994). Rutile-aqueous fluid partitioning of Nb, Ta, Hf, Zr, U and Th: implications for high field strength element depletions in island-arc basalts. *Earth and Planetary Science Letters*, *128*(3-4), pp. 327–339.

Cawthorn, R. G., & O'Hara, M. J. (1976). Amphibole fractionation in calc-alkaline magma genesis. *American Journal of Science*, *276*(3), 309–329.

Cawthorn, R. G., Curran, E. B., & Arculus, R. J. (1973). A petrogenetic model for the origin of the calc-alkaline suite of Grenada, Lesser Antilles. *Journal of Petrology*, *14*(2), 327–337.

Chesner, C. A., & Rose Jr, W. I. (1984). Geochemistry and evolution of the Fuego volcanic

complex, Guatemala. *Journal of Volcanology and Geothermal Research*, *21*(1-2), 25-44.

Coombs, M. L., Eichelberger, J. C., & Rutherford, M. J. (2000). Magma storage and mixing conditions for the 1953–1974 eruptions of Southwest Trident volcano, Katmai National Park, Alaska. *Contributions to Mineralogy and Petrology*, *140*(1), 99–118.

Cox, K. G. (Ed.). (2013). *The interpretation of igneous rocks*. Springer Science & Business Media.

Cruz-Uribe, A. M., Marschall, H. R., Gaetani, G. A., & Le Roux, V. (2018). Generation of alkaline magmas in subduction zones by partial melting of mélange diapirs—An experimental study. *Geology*, *46*(4), 343-346.

Daczko, N. R., & Halpin, J. A. (2009). Evidence for melt migration enhancing recrystallization of metastable assemblages in mafic lower crust, Fiordland, New Zealand. *Journal of Metamorphic Geology*, *27*(2), 167-185.

Dalziel, I. W., Lawver, L. A., Norton, I. O., & Gahagan, L. M. (2013). The Scotia Arc: genesis, evolution, global significance. *Annual Review of Earth and Planetary Sciences*, *41*, 767-793.

DePaolo, D. J. (1981). A neodymium and strontium isotopic study of the Mesozoic calc-alkaline granitic batholiths of the Sierra Nevada and Peninsular Ranges, California. *Journal of Geophysical Research: Solid Earth*, *86*(B11), 10470-10488.

DePaolo, D. J. (1981). Nd isotopic studies: some new perspectives on Earth structure and evolution. *Eos, Transactions American Geophysical Union*, *62*(14), 137-137.

DePaolo, D. J. (1981). Neodymium isotopes in the Colorado Front Range and crust-mantle evolution in the Proterozoic. *Nature*, *291*(5812), 193-196.

DePaolo, D. J. (1981). Trace element and isotopic effects of combined wallrock assimilation and fractional crystallization. *Earth and planetary science letters*, *53*(2), 189-202.

Eichelberger, J. C. (1974). Magma contamination within the volcanic pile: origin of andesite and dacite. *Geology*, *2*(1), 29-33.

Ewart, A., Collerson, K. D., Regelous, M., Wendt, J. I., & Niu, Y. (1998). Geochemical evolution within the Tonga–Kermadec–Lau arc–back-arc systems: the role of varying mantle wedge composition in space and time. *Journal of Petrology*, *39*(3), 331-368.

Falloon, T. J., Green, D. H., Hatton, C. J., & Harris, K. L. (1988). Anhydrous partial melting of a fertile and depleted peridotite from 2 to 30 kb and application to basalt petrogenesis. *Journal of Petrology*, *29*(6), 1257–1282.

Fenner, C. N. (1926). Magmatic problems of the Aleutians. *Eos, Transactions American*

*Geophysical Union*, *7*(1), 124–127.

Francis, D., & Minarik, W. (2008). Aluminum-dependent trace element partitioning in clinopyroxene. *Contributions to Mineralogy and Petrology*, *156*(4), 439-451.

Foley, S. (1992). Vein-plus-wall-rock melting mechanisms in the lithosphere and the origin of potassic alkaline magmas. *Lithos*, *28*(3-6), pp. 435–453.

Foley, S. F., & Pertermann, M. (2021). Dynamic metasomatism experiments investigating the interaction between migrating potassic melt and garnet peridotite. *Geosciences*, *11*(10), 432.

Foley, S. F., Yaxley, G. M., Rosenthal, A., Buhre, S., Kiseeva, E. S., Rapp, R. P., & Jacob, D. E. (2009). The composition of near-solidus melts of peridotite in the presence of CO2 and H2O between 40 and 60 kbar. *Lithos*, pp. *112*, 274–283.

Gest, D. E., & McBirney, A. R. (1979). Genetic relations of shoshonitic and absarokitic magmas, Absaroka Mountains, Wyoming. *Journal of Volcanology and Geothermal Research*, *6*(1-2), 85-104.

Ghiorso, M. S., & Sack, R. O. (1995). Chemical mass transfer in magmatic processes IV. A revised and internally consistent thermodynamic model for interpolating liquid-solid equilibria in magmatic systems at elevated temperatures and pressures. *Contributions to Mineralogy and Petrology*, *119*(2), 197–212.

Ghiorso, M. S., Hirschmann, M. M., Reiners, P. W., & Kress III, V. C. (2002). The pMELTS: A revision of MELTS for improved calculation of phase relations and major element partitioning related to partial melting of the mantle to 3 GPa. *Geochemistry, Geophysics, Geosystems*, *3*(5), 1-35.

Green, D. H. (1973). Conditions of melting of basanite magma from garnet peridotite. *Earth and planetary science letters*, *17*(2), 456–465.

Green, D. H. (1973). Contrasted melting relations in a pyrolite upper mantle under the mid-oceanicridge, stable crust and island arc environments. *Tectonophysics*, *17*(3), 285–297.

Green, D. H. (1973). Experimental melting studies on a model upper mantle composition at high pressure under water-saturated and water-undersaturated conditions. *Earth and Planetary Science Letters*, *19*(1), 37–53.

Green, D. H. (1976). Experimental testing of" equilibrium" partial melting of peridotite under water-saturated, high-pressure conditions. *The Canadian Mineralogist*, *14*(3), 255–268.

Green, T. H. (1980). Island arc and continent-building magmatism—A review of petrogenic

models based on experimental petrology and geochemistry. *Tectonophysics*, *63*(1-4), pp. 367–385.

Green, T. H. (1980). Island arc and continent-building magmatism—A review of petrogenic models based on experimental petrology and geochemistry. *Tectonophysics*, *63*(1-4), pp. 367–385.

Grove, T. L., & Baker, M. B. (1984). Phase equilibrium controls the tholeiitic versus calc-alkaline differentiation trends. *Journal of Geophysical Research: Solid Earth*, *89*(B5), 3253-3274.

Grove, T. L., Elkins-Tanton, L. T., Parman, S. W., Chatterjee, N., Müntener, O., & Gaetani, G. A. (2003). Fractional crystallisation and mantle-melting controls on calc-alkaline differentiation trends. *Contributions to Mineralogy and Petrology*, *145*(5), 515-533.

Grove, T. L., Kinzler, R. J., & Bryan, W. B. (1992). Fractionation of mid-ocean ridge basalt (MORB). *Washington DC American Geophysical Union Geophysical Monograph Series*, *71*, 281-310.

Grove, T. L., Till, C. B., & Krawczynski, M. J. (2012). The role of H 2 O in subduction zone magmatism. *Annual Review of Earth and Planetary Sciences*, *40*(413), 2012.

Gupta, A. K., YAGI, K., Hariya, Y., & Onuma, K. (1976). Experimental investigations on some synthetic leucite rocks under water vapour pressures. *Proceedings of the Japan Academy*, *52*(9), 469-472.

Gust, D. A., & Perfit, M. R. (1987). Phase relations of a high-Mg basalt from the Aleutian island arc: implications for primary island arc basalts and high-Al basalts. *Contributions to Mineralogy and Petrology*, *97*(1), 7–18.

Halliday, A. N., Davidson, J. P., Hildreth, W., & Holden, P. (1991). Modelling the petrogenesis of high Rb/Sr silicic magmas. *Chemical Geology*, *92*(1-3), pp. 107–114.

Harker, A. (1909). *The natural history of igneous rocks*. Methuen & Company.

Hawkesworth, C. J., Gallagher, K., Hergt, J. M., & McDermott, F. (1994). Destructive plate margin magmatism: Geochemistry and melt generation. *Lithos*, *33*(1-3), pp. 169–188.

Hawkesworth, C. J., Hergt, J. M., McDermott, F., & Ellam, R. M. (1991). Destructive margin magmatism and the contributions from the mantle wedge and subducted crust. *Australian Journal of Earth Sciences*, *38*(5), 577–594.

Hensen, B. J., & Green, D. H. (1973). Experimental study of the stability of cordierite and garnet in pelitic compositions at high pressures and temperatures. *Contributions to Mineralogy and*

*Petrology*, *38*(2), 151-166.

Hildreth, W. (1981). Gradients in silicic magma chambers: implications for lithospheric magmatism. *Journal of Geophysical Research: Solid Earth*, *86*(B11), 10153–10192.

Hildreth, W., & Moorbath, S. (1988). Crustal contributions to arc magmatism in the Andes of central Chile. *Contributions to mineralogy and petrology*, *98*(4), 455–489.

Hirschmann, M. M., & Stolper, E. M. (1996). A possible role for garnet pyroxenite in the origin of the "garnet signature" in MORB. *Contributions to Mineralogy and Petrology*, *124*(2), 185-208.

Hofmann, A. W., & White, W. M. (1982). Mantle plumes from ancient oceanic crust. *Earth and Planetary Science Letters*, *57*(2), 421-436.

Holbrook, W. S., & Kelemen, P. B. (1993). Large igneous province on the US Atlantic margin and implications for magmatism during continental breakup. Nature, 364(6436), 433–436.

Howie, R. A., Zussman, J., & Deer, W. (1992). *An introduction to the rock-forming minerals* (p. 696). London, UK: Longman.

Iddings, J. P. (1895). Absarokite-shoshonite-banakite series. *The Journal of Geology*, *3*(8), 935–959.

Irving, A. J., & Green, D. H. (1976). Geochemistry and petrogenesis of the Newer Basalts of Victoria and South Australia. *Journal of the Geological Society of Australia*, *23*(1), 45–66.

Jakeš, P., & White, A. J. R. (1970). K/Rb ratios of rocks from island arcs. *Geochimica et Cosmochimica Acta*, *34*(8), 849-856.

Jaques, A. L., & Green, D. H. (1980). Anhydrous melting of peridotite at 0–15 kb pressure and the genesis of tholeiitic basalts. *Contributions to mineralogy and petrology*, *73*(3), 287-310.

Joplin, G. A. (1968). The shoshonite association: a review. *Journal of the Geological Society of Australia*, *15*(2), 275-294.

Kay, R. W. (1980). Volcanic arc magmas: implications of a melting-mixing model for element recycling in the crust-upper mantle system. *The Journal of Geology*, *88*(5), 497–522.

Kay, S. M., & Kay, R. W. (1985). Role of crystal cumulates and the oceanic crust in the formation of the lower crust of the Aleutian arc. *Geology*, *13*(7), 461-464.

Kelemen, P. B., Shimizu, N., & Dunn, T. (1993). Relative depletion of niobium in some arc magmas and the continental crust: partitioning of K, Nb, La and Ce during melt/rock reaction in the upper mantle. *Earth and Planetary Science Letters*, *120*(3-4), 111-134.

Kinzler, R. J., & Grove, T. L. (1992). Primary magmas of mid-ocean ridge basalts 1. Experiments and methods. *Journal of Geophysical Research: Solid Earth*, *97*(B5), 6885-6906.

Kogiso, T., Hirschmann, M. M., & Pertermann, M. (2004). High-pressure partial melting of mafic lithologies in the mantle. *Journal of Petrology*, *45*(12), 2407-2422.

Kogiso, T., Hirschmann, M. M., & Pertermann, M. (2004). High-pressure partial melting of mafic lithologies in the mantle. *Journal of Petrology*, *45*(12), 2407-2422.

Kogiso, T., Hirschmann, M. M., & Reiners, P. W. (2004). Length scales of mantle heterogeneities and their relationship to ocean island basalt geochemistry. *Geochimica et Cosmochimica Acta*, *68*(2), 345-360.

Kogiso, T., Omori, S., & Maruyama, S. (2009). Magma genesis beneath Northeast Japan arc: a new perspective on subduction zone magmatism. *Gondwana Research*, *16*(3-4), 446-457.

Krienitz, M. S., Haase, K. M., Mezger, K., & Shaikh-Mashail, M. A. (2007). Magma genesis and mantle dynamics at the Harrat Ash Shamah volcanic field (southern Syria). *Journal of Petrology*, *48*(8), 1513-1542.

Lambart, S., Laporte, D., & Schiano, P. (2009). An experimental study of pyroxenite partial melts at 1 and 1.5 GPa: Implications for the major-element composition of Mid-Ocean Ridge Basalts. *Earth and Planetary Science Letters*, *288*(1-2), 335-347.
Lambart, S., Laporte, D., & Schiano, P. (2009). An experimental study of pyroxenite partial melts at 1 and 1.5 GPa: Implications for the major-element composition of Mid-Ocean Ridge Basalts. *Earth and Planetary Science Letters*, *288*(1-2), 335-347.

Lambart, S., Laporte, D., & Schiano, P. (2009). An experimental study of focused magma transport and basalt–peridotite interactions beneath mid-ocean ridges: implications for the generation of primitive MORB compositions. *Contributions to Mineralogy and Petrology*, *157*(4), 429-451.

Lambart, S., Laporte, D., & Schiano, P. (2013). Markers of the pyroxenite contribution in the major-element compositions of oceanic basalts: Review of the experimental constraints. *Lithos*, *160*, 14-36.

Lambart, S., Laporte, D., Provost, A., & Schiano, P. (2012). Fate of pyroxenite-derived melts in the peridotitic mantle: thermodynamic and experimental constraints. *Journal of Petrology*, *53*(3), 451-476.

Langmuir, C. H., Klein, E. M., & Plank, T. (1992). Petrological systematics of mid-ocean ridge basalts: constraints on melt generation beneath ocean ridges. *Mantle flow and melt generation*

*at mid-ocean ridges*, 183-280.

LaTourrette, T., Hervig, R. L., & Holloway, J. R. (1995). Trace element partitioning between amphibole, phlogopite, and basanite melt. *Earth and Planetary Science Letters*, *135*(1-4), 13-30.

Le Roux, V., Bodinier, J. L., Alard, O., O'Reilly, S. Y., & Griffin, W. L. (2009). Isotopic decoupling during porous melt flow: a case-study in the Lherz peridotite. *Earth and Planetary Science Letters*, *279*(1-2), pp. 76–85.

Leeman, W. P. (2020). Old/new subduction zone paradigms are seen from the cascades. *Frontiers in Earth Science*, *8*, 535879.

Longerich, H. P., Jackson, S. E., & Günther, D. (1996). Inter-laboratory note. Laser ablation inductively coupled plasma mass spectrometric transient signal data acquisition and analyte concentration calculation. *Journal of analytical atomic spectrometry*, *11*(9), 899-904.

Maitre, L. E. (1989). A classification of igneous rocks and glossary of terms. *Recommendations of the international union of geological sciences subcommission on the systematics of igneous rocks*, *193*.

Mattinson, J. M., Fink, L. K., & Hopson, C. A. (1980). Geochronologic and isotopic study of the La Désirade island basement complex: Jurassic oceanic crust in the Lesser Antilles? *Contributions to Mineralogy and Petrology*, *71*(3), 237–245.

McBirney, A. R., Taylor, H. P., & Armstrong, R. L. (1987). Paricutin re-examined: a classic example of crustal assimilation in calc-alkaline magma. *Contributions to Mineralogy and Petrology*, *95*(1), 4–20.

McInnes, B. I., & Cameron, E. M. (1994). Carbonated, alkaline hybridizing melts from a sub-arc environment: Mantle wedge samples from the Tabar-Lihir-Tanga-Feni arc, Papua New Guinea. *Earth and Planetary Science Letters*, *122*(1-2), pp. 125–141.

McKibbin, S. J., Landenberger, B., & Fanning, C. M. (2017). First magmatism in the New England Batholith, Australia: forearc and arc–back-arc components in the Bakers Creek Suite gabbros. *Solid Earth*, *8*(2), 421-434.

Morgan, Z., & Liang, Y. (2005). An experimental study of the kinetics of lherzolite reactive dissolution with applications to melt channel formation. *Contributions to Mineralogy and Petrology*, *150*(4), 369–385.

Morrison, G. W. (1980). Characteristics and tectonic setting of the shoshonite rock association. *Lithos*, *13*(1), 97–108.

Morse, S. A. (1980). *Basalts and phase diagrams: an introduction to the quantitative use of phase diagrams in igneous petrology* (p. 493). New York: Springer-Verlag.

Nicholls, I. A., & Ringwood, A. E. (1973). Effect of water on olivine stability in tholeiites and the production of silica-saturated magmas in the island-arc environment. *The Journal of Geology*, *81*(3), 285–300.

Osborn, E. F. (1959). Role of oxygen pressure in the crystallisation and differentiation of basaltic magma. *American Journal of Science*, *257*(9), 609–647.

Pawley, A. R., & Holloway, J. R. (1993). Water sources for subduction zone volcanism: New experimental constraints. *Science*, *260*(5108), 664–667.

Pawley, A. R., McMillan, P. F., & Holloway, J. R. (1993). Hydrogen in stishovite, with implications for mantle water content. *Science*, *261*(5124), 1024–1026.

Peacock, M. A. (1931). Classification of igneous rock series. *The Journal of Geology*, *39*(1), 54–67.

Peacock, S. A. (1990). Fluid processes in subduction zones. *Science*, *248*(4953), 329–337.

Pearce, J. A., Stern, R. J., Bloomer, S. H., & Fryer, P. (2005). Geochemical mapping of the Mariana arc-basin system: Implications for the nature and distribution of subduction components. *Geochemistry, geophysics, geosystems*, *6*(7).

Pec, M., Holtzman, B. K., Zimmerman, M. E., & Kohlstedt, D. L. (2020). Influence of lithology on reactive melt flow channelisation. *Geochemistry, Geophysics, Geosystems*, *21*(8), e2020GC008937.

Pec, M., Holtzman, B. K., Zimmerman, M. E., & Kohlstedt, D. L. (2017). Reaction infiltration instabilities in mantle rocks: an experimental investigation. *Journal of Petrology*, *58*(5), 979-1003.

Pec, M., Holtzman, B. K., Zimmerman, M., & Kohlstedt, D. L. (2015). Reaction infiltration instabilities in experiments on partially molten mantle rocks. *Geology*, *43*(7), 575-578.

Peccerillo, A., & Taylor, S. R. (1976). Geochemistry of Eocene calc-alkaline volcanic rocks from the Kastamonu area, northern Turkey. *Contributions to mineralogy and petrology*, *58*(1), 63-81.

Peng, Z. X., Mahoney, J., Hooper, P., Harris, C., & Beane, J. (1994). A role for the lower continental crust in flood basalt genesis? Isotopic and incompatible element study of the lower six formations of the western Deccan Traps. *Geochimica et Cosmochimica Acta*, *58*(1), 267-288.

Pertermann, M., & Hirschmann, M. M. (2003). Anhydrous partial melting experiments on

MORB-like eclogite: phase relations, phase compositions and mineral–melt partitioning of major elements at 2–3 GPa. *Journal of Petrology*, *44*(12), 2173-2201.

Pertermann, M., & Hirschmann, M. M. (2003). Partial melting experiments on a MORB-like pyroxenite between 2 and 3 GPa: Constraints on the presence of pyroxenite in basalt source regions from solidus location and melting rate. *Journal of Geophysical Research: Solid Earth*, *108*(B2).

Plank, T., & Langmuir, C. H. (1992). Effects of the melting regime on the composition of the oceanic crust. *Journal of Geophysical Research: Solid Earth*, *97*(B13), 19749-19770.

Poli, S., & Schmidt, M. W. (1995). H2O transport and release in subduction zones: experimental constraints on basaltic and andesitic systems. *Journal of Geophysical Research: Solid Earth*, *100*(B11), 22299-22314.

Reagan, M. K., & Gill, J. B. (1989). Coexisting calcalkaline and high-niobium basalts from Turrialba Volcano, Costa Rica: Implications for residual titanates in arc magma sources. *Journal of Geophysical Research: Solid Earth*, *94*(B4), pp. 4619–4633.

Reynolds, J. R., Langmuir, C. H., Bender, J. F., Kastens, K. A., & Ryan, W. B. (1992). Spatial and temporal variability in the geochemistry of basalts from the East Pacific Rise. *Nature*, *359*(6395), 493–499.

Ringwood, A. E. (1982). Phase transformations and differentiation in the subducted lithosphere: Implications for mantle dynamics, basalt petrogenesis, and crustal evolution. *The Journal of Geology*, *90*(6), 611–643.

Rollinson, H. R. (2014). *Using geochemical data: evaluation, presentation, interpretation*. Routledge.

Scambelluri, M., & Philippot, P. (2001). Deep fluids in subduction zones. *Lithos*, *55*(1-4), 213-227.

Schmidt, M. W., & Poli, S. (1998). Experimentally based water budgets for dehydrating slabs and consequences for arc magma generation. *Earth and Planetary Science Letters*, *163*(1-4), 361-379.

Schmidt, M. W., & Poli, S. (2004). Magmatic epidote. *Reviews in Mineralogy and Geochemistry*, *56*(1), 399-430.

Schreyer, W. (1988). Experimental studies on metamorphism of crustal rocks under mantle pressures. *Mineralogical Magazine*, *52*(364), 1–26.

Schreyer, W. (1988). Subduction of continental crust to mantle depths: Petrological evidence. *Episodes Journal of International Geoscience*, *11*(2), 97–104.

Sekine, T., & Wyllie, P. J. (1982). Synthetic systems for modelling hybridisation between hydrous siliceous magmas and peridotite in subduction zones. *The Journal of Geology*, *90*(6), 734-741.
Sekine, T., & Wyllie, P. J. (1982). Synthetic systems for modelling hybridisation between hydrous siliceous magmas and peridotite in subduction zones. *The Journal of Geology*, *90*(6), 734-741.

Sekine, T., & Wyllie, P. J. (1982). The system granite-peridotite-$H_2O$ at 30 kbar, with applications to hybridisation in subduction zone magmatism. *Contributions to Mineralogy and Petrology*, *81*(3), 190-202.

Sekine, T., & Wyllie, P. J. (1983). Experimental simulation of mantle hybridisation in subduction zones. *The Journal of Geology*, *91*(5), 511-528.

Sheth, H. C., Torres-Alvarado, I. S., & Verma, S. P. (2002). What is the" calc-alkaline rock series"? *International Geology Review*, *44*(8), 686-701.

Sorbadere, F., Médard, E., Laporte, D., & Schiano, P. (2013). Experimental melting of hydrous peridotite–pyroxenite mixed sources: Constraints on the genesis of silica-undersaturated magmas beneath volcanic arcs. *Earth and Planetary Science Letters*, *384*, 42-56.
Sorbadere, F., Médard, E., Laporte, D., & Schiano, P. (2013). Experimental melting of hydrous peridotite–pyroxenite mixed sources: Constraints on the genesis of silica-undersaturated magmas beneath volcanic arcs. *Earth and Planetary Science Letters*, *384*, 42-56.

Sorbadere, F., Schiano, P., & Métrich, N. (2013). Constraints on the origin of nepheline-normative primitive magmas in island arcs inferred from olivine-hosted melt inclusion compositions. *Journal of Petrology*, *54*(2), 215–233.

Sorbadere, F., Schiano, P., Métrich, N., & Bertagnini, A. (2013). Small-scale coexistence of island-arc-and enriched-MORB-type basalts in the central Vanuatu arc. *Contributions to Mineralogy and Petrology*, *166*(5), 1305-1321.

Sorbadere, F., Schiano, P., Metrich, N., Medard, E., & Laporte, D. (2013, December). Constraints on the origin of silica-undersaturated arc magmas inferred from melt inclusions and experimental melting of t h e peridotite-pyroxenite mixed source. In *AGU Fall Meeting Abstracts* (Vol. 2013, pp. V23D-04).

Soustelle, V., & Tommasi, A. (2010). Seismic properties of the supra-subduction mantle: Constraints from peridotite xenoliths from the Avacha volcano, southern Kamchatka.

*Geophysical Research Letters*, *37*(13).

Soustelle, V., Tommasi, A., Bodinier, J. L., Garrido, C. J., & Vauchez, A. (2009). Deformation and reactive melt transport in the mantle lithosphere above a large-scale partial melting domain: the Ronda Peridotite Massif, Southern Spain. *Journal of Petrology*, *50*(7), 1235-1266.

Soustelle, V., Tommasi, A., Demouchy, S., & Ionov, D. A. (2010). Deformation and fluid-rock interaction in the supra-subduction mantle: microstructures and water contents in peridotite xenoliths from the Avacha Volcano, Kamchatka. *Journal of Petrology*, *51*(1-2), 363-394.

Soustelle, V., Walte, N. P., Manthilake, M. G. M., & Frost, D. J. (2014). Melt migration and melt-rock reactions in the deforming Earth's upper mantle: Experiments at high pressure and temperature. *Geology*, *42*(1), 83-86.

Stern, R. J. (2002). Subduction zones. *Reviews of Geophysics*, *40*(4), 3–1.

Stracke, A. (2012). Earth's heterogeneous mantle: A product of convection-driven interaction between crust and mantle. *Chemical Geology*, pp. *330*, 274–299.

Sudo, A., & Tatsumi, Y. (1990). Phlogopite and K-amphibole in the upper mantle: Implication for magma genesis in subduction zones. *Geophysical Research Letters*, *17*(1), 29-32.

Tatsumi, Y. (1989). Migration of fluid phases and genesis of basalt magmas in subduction zones. *Journal of Geophysical Research: Solid Earth*, *94*(B4), 4697–4707.

Tatsumi, Y., Otofuji, Y. I., Matsuda, T., & Nohda, S. (1989). Opening of the Sea of Japan back-arc basin by asthenospheric injection. *Tectonophysics*, *166*(4), 317-329.

Tsvetkov, A. A. (1991). Magmatism of the westernmost (Komandorsky) segment of the Aleutian Island Arc. *Tectonophysics*, *199*(2-4), 289-317.

Turner, S. J., Langmuir, C. H., Katz, R. F., Dungan, M. A., & Escrig, S. (2016). Parental arc magma compositions are dominantly controlled by mantle-wedge thermal structure. *Nature Geoscience*, *9*(10), 772–776.

Turner, S., Bourdon, B., & Gill, J. (2003). Insights into magma genesis at convergent margins from U-series isotopes. *Reviews in Mineralogy and Geochemistry*, *52*(1), 255-315.

Ulmer, P., & Trommsdorff, V. (1995). Serpentine stability to mantle depths and subduction-related magmatism. *Science*, *268*(5212), 858-861.

White, W. M., & Hofmann, A. W. (1982). Sr and Nd isotope geochemistry of oceanic basalts and mantle evolution. *Nature*, *296*(5860), 821-825.

White, W. M., Hofmann, A. W., & Puchelt, H. (1987). Isotope geochemistry of Pacific mid-ocean ridge basalt. *Journal of Geophysical Research: Solid Earth*, *92*(B6), 4881-4893.

Wilcox, R. E. (1954). *Petrology of Parícutin Volcano Mexico* (No. 965). US Government Printing Office.

Wunder, B., & schreyer, w. (1992). Metastability of the 10-Å Phase in the $MgO–SiO_2–H_2O$ (MSH) system. What about hydrous MSH phases in subduction zones? *Journal of Petrology*, *33*(4),877-889.

Wyllie, P. J., & Sekine, T. (1982). The formation of mantle phlogopite in subduction zone hybridisation. *Contributions to Mineralogy and Petrology*, *79*(4), 375-380.

Yang, J. H., Wu, F. Y., Wilde, S. A., Chen, F., Liu, X. M., & Xie, L. W. (2008). Petrogenesis of an alkali syenite–granite–rhyolite suite in the Yanshan Fold and Thrust Belt, Eastern North China Craton: geochronological, geochemical and Nd–Sr–Hf isotopic evidence for lithospheric thinning. *Journal of Petrology*, *49*(2), 315-351.

Yoder Jr, H. S. (1973). Contemporaneous basaltic and rhyolitic magmas. *American Mineralogist: Journal of Earth and Planetary Materials*, *58*(3-4_Part_1), pp. 153–171.

Yu, Z. F., Peng, Q. M., Zhao, Z., Wang, P. A., Xia, Y., Wang, Y. Q., & Wang, H. (2020). Geochronology, geochemistry, and geodynamic relationship of the mafic dykes and granites in the Qianlishan Complex, South China. *Minerals*, *10*(12), 1069.

Zheng, J., Xiong, Q., Zhao, Y., & Li, W. (2019). Subduction-zone peridotites and their records of crust-mantle interaction. *Science China Earth Sciences*, *62*(7), 1033–1052.

Zheng, Y. F. (2019). Subduction zone geochemistry. *Geoscience Frontiers*, *10*(4), 1223–1254.

Zimmer, M. M., Plank, T., Hauri, E. H., Yogodzinski, G. M., Stelling, P., Larsen, J., & Nye, C. J. (2010). The role of water in generating the calc-alkaline trend: new volatile data for Aleutian magmas and a new tholeiitic index. *Journal of Petrology*, *51*(12), 2411-2444.

Zimmer, M. M., Plank, T., Hauri, E. H., Yogodzinski, G. M., Stelling, P., Larsen, J., ... & Nye, C. J. (2010). The role of water in generating the calc-alkaline trend: new volatile data for Aleutian magmas and a new tholeiitic index. *Journal of Petrology*, *51*(12), 2411-2444.

Zimmer, M. M., Plank, T., Hauri, E. H., Yogodzinski, G. M., Stelling, P., Larsen, J., ... & Nye, C. J. (2010). The role of water in generating the calc-alkaline trend: new volatile data for Aleutian magmas and a new tholeiitic index. *Journal of Petrology*, *51*(12), 2411-2444.

Zindler, A., & Hart, S. (1986). Chemical geodynamics. *Annual review of earth and planetary sciences*, *14*, 493-571.

# Appendix

In the early stages of our study, we started the melt-rock reactions using noble metal capsules made of $Ag_{70}Pd_{30}$ for high-pressure experiments. The samples were arranged in three layers, with the bottom layer being the initial melt and the top layer being the carbon trap. A layer of Peridotite and Gabbro rock was sandwiched between these two layers, allowing the initial melt to migrate through the rock layer and collect in the carbon trap.

The purpose of this section is to present the experimental details of the melt-rock reactions between the phlogopite-pyroxenite melt and mantle wedge peridotite and lower crustal gabbro using the $Ag_{70}Pd_{30}$ noble metal capsule, together with some microscopic images, BSE images, along with a few mineralogical and chemical maps as well.

| Experimental Run | Material used | Pressure | Temp. | Hours | Phases occurred |
|---|---|---|---|---|---|
| Melt-peridotite reaction | Capsule- $Ag_{70}Pd_{30}$ Pyroxenite+ peridotite+ vitreous carbon trap | 1.5 GPa | 1200$^{o}$ C | 28 Hours | Rich in diopside and phlogopite. Rock minerals that have recrystallised include forsterite. |
| Melt-gabbro powder reaction | Capsule- $Ag_{70}Pd_{30}$ Pyroxenite+ gabbro (powder)+ vitreous carbon trap | 1.5 GPa | 1100$^{o}$ C | 28 Hours | Rich in diopside, phlogopite ± garnet. Rock minerals that have recrystallised include plagioclase and diopside. |
| Melt-gabbro core reaction | Capsule- $Au_{70}Pd_{30}$ Pyroxenite+ gabbro core+ vitreous carbon trap | 1.5 GPa | 1100$^{o}$ C | 28Hours | Plagioclase, Garnet, diopside, enstatite. Rock minerals that have recrystallised include plagioclase and diopside. |

*Table 1: Details of experimental run conditions in $Ag_{70}Pd_{30}$ capsule for melt-peridotite and melt-gabbro reaction experiments.*

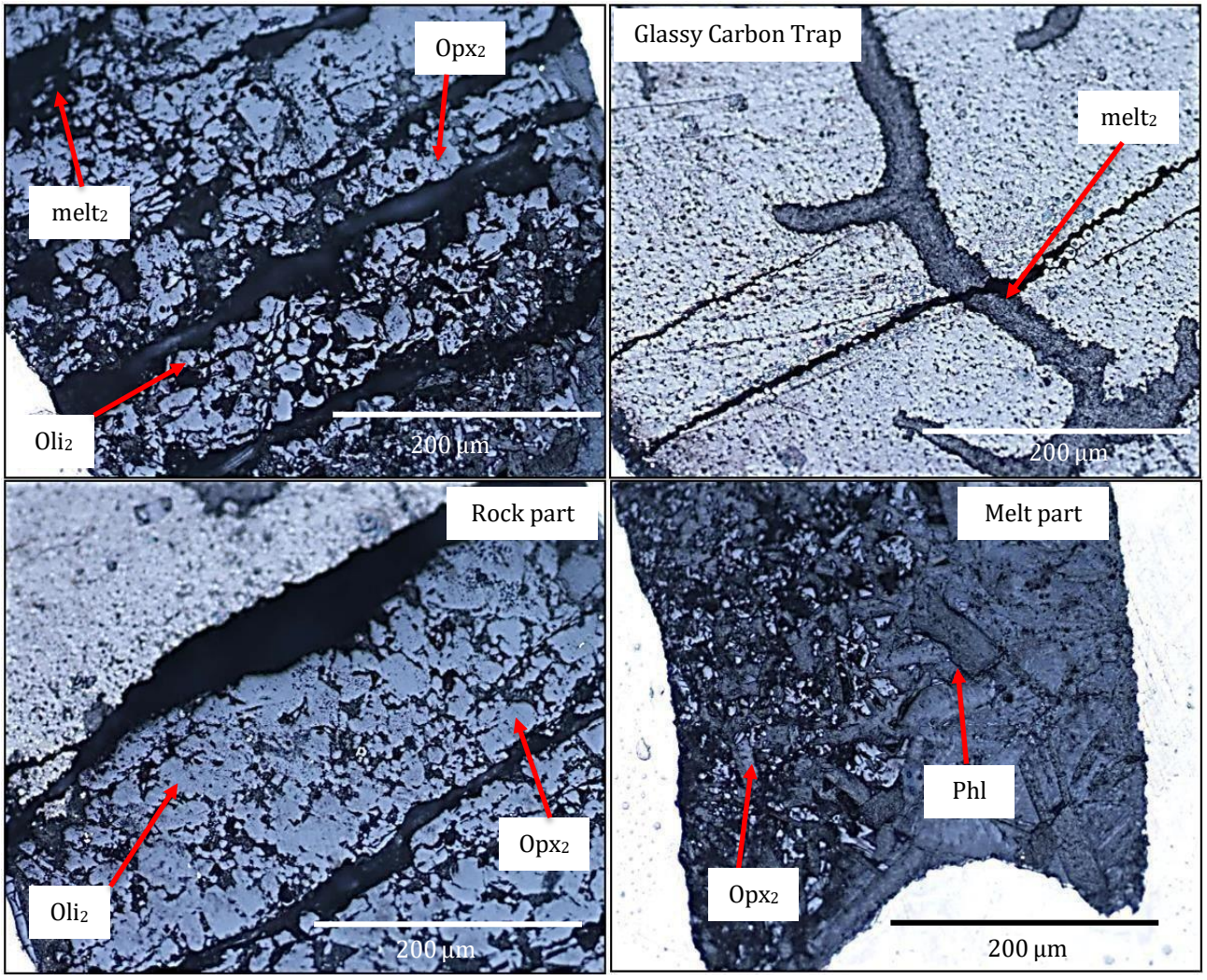


*Figure 1: BSE Images of the melt-rock experimental reactions in $Au_{70}Pd_{30}$ capsule at the pressure of 1.5 GPa and $1200^0$ C for melt-peridotite reactions in the mantle wedge.*

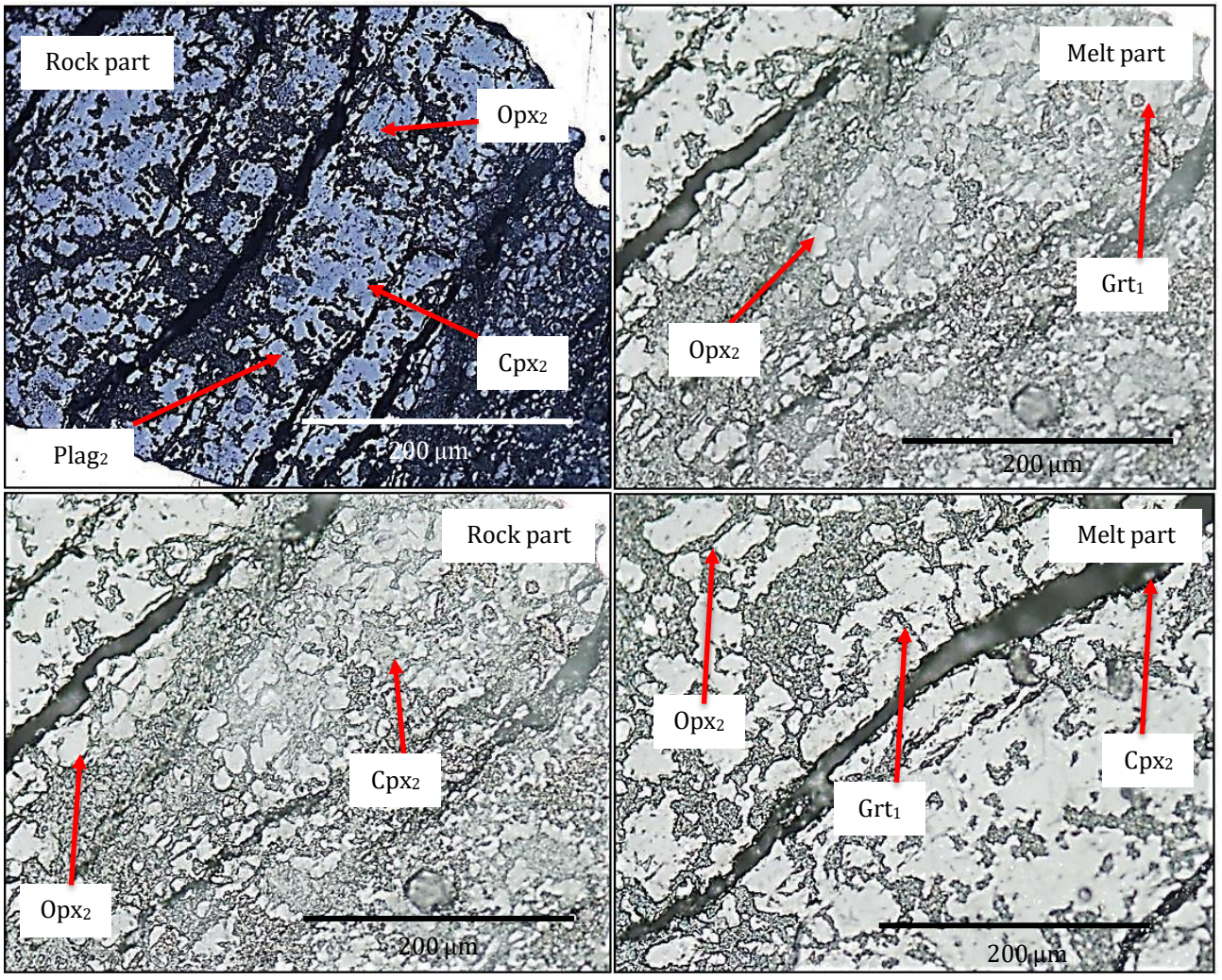


*Figure 2: BSE Images of the melt-rock experimental reactions in $Au_{70}Pd_{30}$ capsule at the pressure of 1.5 GPa and $1150^0$ C for melt-gabbro reactions in the lower crust.*


*Figure 3: Mineralogical maps of melt-rock reactions obtained from an FEI Teneo Field Emission Scanning Electron Microscop e (SEM) with the Nanomin software. (A) mineralogical mapsof melt-peridotite reaction comprise annite (iron-rich end-member of biotite), phlogopite (magnesium-rich end-member of biotite), clinopyroxene, orthopyroxene and olivine, (B) mineralogical maps of melt-gabbro reaction comprise plagioclase, annite, phlogopite, clinopyroxene, orthopyroxene and garnet.*

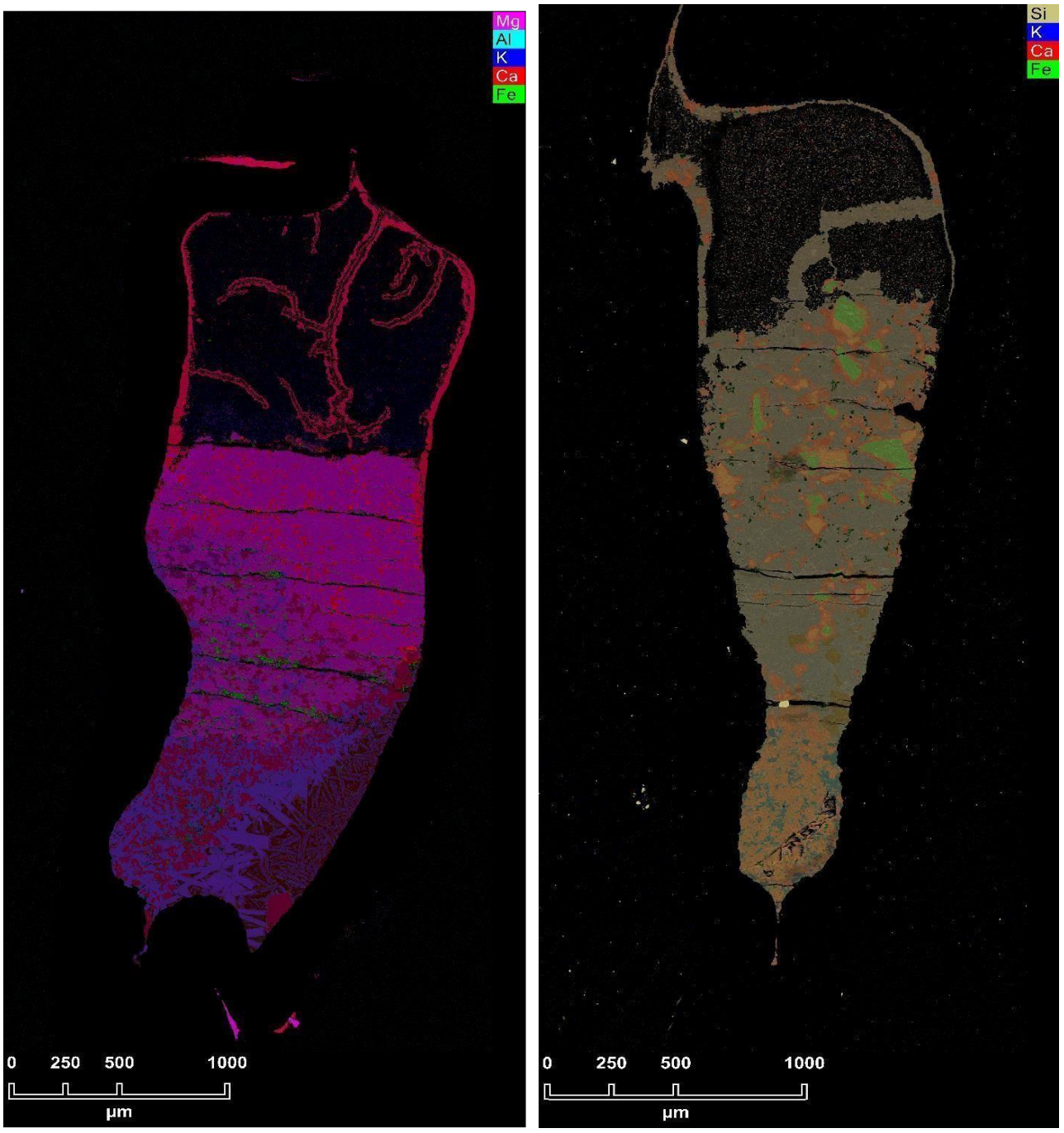


*Figure 4: Chemical maps of melt-rock reactions obtained from an FEI Teneo Field Emission Scanning Electron Microscope (SEM) with the NanoMin software. (A) chemical maps of the melt-peridotite reaction including Mg, Al, Ca, K, and Fe oxides, (B) chemical maps of the melt-gabbroreaction including Si, K, Ca, and Fe oxides.*